Research Square

Preprints are preliminary reports that have not undergone peer review.
They should not be considered conclusive, used to inform clinical practice,
or referenced by the media as validated information.

Hsa_circ_0001944 promotes colorectal cancer progression through the miR- 665/IGF2BP1/PKM2 axis-mediated glycolysis

Ruhang Zhou
First Affiliated Hospital of Anhui Medical University
Xudong Jiang
Second Affiliated Hospital of Anhui Medical University
Jun Lei
Second Affiliated Hospital of Anhui Medical University
Zhaibiao Wang
The Affiliated Bozhou Hospital of Anhui Medical University
Xiaosi Hu
Anhui No.2 Provincial People's Hospital
Aman Xu
xuaman@ahmu.edu.cn

First Affiliated Hospital of Anhui Medical University

Research Article

Keywords: Hsa_circ_0001944, colorectal cancer, miR-665, IGF2BP1, aerobic glycolysis

Posted Date: August 24th, 2026

DOI: https://doi.org/10.21203/rs.3.rs-10603551/v1

License: This work is licensed under a Creative Commons Attribution 4.0 International License.
Read Full License

Additional Declarations: No competing interests reported.

Version of Record: A version of this preprint was published at European Journal of Medical Research on September 22nd, 2026. See the published version at https://doi.org/10.1186/s40001-026-05239-2.

Hsa_circ_0001944 promotes colorectal cancer progression through the miR-665/IGF2BP1/PKM2 axis-mediated glycolysis

Ruhang Zhou[1,2#], Xudong Jiang [2#], Jun Lei[2,3#], Zhaibiao Wang[4], Xiaosi Hu[5]✉**M.D.**, Aman Xu[1]✉**M.D.**

Ruhang Zhou:zhouruhang2025@fy.ahmu.edu.cn

Xudong Jiang: jiangxudong2025@fy.ahmu.edu.cn

Jun Lei:leijun0701@126.com

Zaibiao Wang:wangzblw@163.com

Xiaosi Hu: surgeryhxs@163.com

Institutions and Affiliations: [1]Department of General Surgery, The First Affiliated Hospital of Anhui Medical University, 28 Jixi Road, Heifei, China, 230001. [2] Department of General Surgery, The Second Affiliated Hospital of Anhui Medical University, No. 678 Furong Road, Economic and Technical Development Zone, Heifei, China, 230601. [3] Department of General Surgery, Affiliated Hospital of West Anhui Health Vocational College, No. 406, Gaocheng Middle Road, Jin'an District, Luan, China,237000. [4] Department of General Surgery, The Affiliated Bozhou Hospital of Anhui Medical University, No. 616, Duzhong Road, Bozhou Economic Development Zone, Bozhou, China,236800.[5] Department of General Surgery, Anhui No.2 Provincial People's Hospital, 1868 Tangshan Road, North Second Ring Road, Hefei, Anhui, China, 230041

✉**Corresponding Authors:**

Aman Xu, Ph.D. M.D.

Email: xuaman@ahmu.edu.cn

Telephone: +8613705695470

Address: 28 Jixi Road, Hefei, Anhui, China, 230001

Xiaosi Hu, MD

Email: surgeryhxs@163.com

Telephone: +86 15155706076

Address: 1868 Tangshan Road, North Second Ring Road, Hefei, Anhui, China, 230041

Ruhang Zhou, Xudong Jiang and Jun Lei contributed equally to this work.

Abstract

Colorectal cancer (CC) is a highly heterogeneous malignancy with a poor prognosis. Although previous studies have suggested that circular RNA hsa_circ_0001944 is involved in CC progression, its precise biological role remains unclear. This study aimed to investigate the function and underlying mechanism of hsa_circ_0001944 in CC. Fluorescence in situ hybridization (FISH) and real-time quantitative PCR (RT-qPCR) were used to assess the expression and subcellular localization of hsa_circ_0001944 in CC tissues and cell lines. Functional assays, including Cell Counting Kit-8 (CCK-8), ethynyl-2'-deoxyuridine (EdU) incorporation, Transwell migration assays, and xenograft tumor models, were performed to evaluate its biological effects. Mechanistic investigations were conducted using bioinformatics analysis, dual-luciferase reporter assays, and rescue experiments. Cellular metabolism was assessed using Seahorse extracellular flux analysis to measure extracellular acidification rate (ECAR) and oxygen consumption rate (OCR). The results showed that hsa_circ_0001944 was significantly upregulated in CC tissues and cell lines. Knockdown of hsa_circ_0001944 significantly inhibited cell proliferation, migration, and tumor growth in vitro and in vivo. Mechanistically, hsa_circ_0001944 acted as a molecular sponge for miR-665, thereby regulating insulin-like growth factor 2 mRNA-binding protein 1 (IGF2BP1). Rescue experiments demonstrated that miR-665 inhibition or IGF2BP1 overexpression reversed the suppressive effects induced by hsa_circ_0001944 silencing. Furthermore, IGF2BP1 overexpression restored aerobic glycolysis, as evidenced by increased ECAR and decreased OCR, and regulated pyruvate kinase M2 (PKM2) expression. In conclusion, hsa_circ_0001944 promotes colorectal cancer progression by regulating the miR-665/IGF2BP1/PKM2 axis and metabolic reprogramming.

Running title: circ_0001944 Drives CRC via miR-665/IGF2BP1 Axis

Keywords: Hsa_circ_0001944; colorectal cancer; miR-665; IGF2BP1, aerobic glycolysis

Introduction

Colorectal cancer (CC) is the third most common cancer and therefore poses a challenge to the healthcare system worldwide [1, 2]. Recent statistics show that in 2020, there were over 1.9 million new cancer patients, and the cancer-related mortality reached 93,000, accounting for ~10% of all cancers and 9.4% of cancer-related mortality [3]. Although early CC detection can help reduce the incidence and mortality rates, the lack of obvious early symptoms means that most CCs are diagnosed at advanced stages, which limits the opportunity for effective treatments. New therapeutic targets and biomarkers are needed to achieve effective early CC diagnosis, precision medical treatments, and monitoring, thereby improving prognosis [4].

The human genome contains large amounts of non-coding RNAs (ncRNAs), and correlations between ncRNAs and human traits are extremely useful in research, particularly in cancer studies. Circular RNAs (circRNAs), long ncRNAs, and microRNAs (miRs) are important members of the ncRNA family. CircRNAs have a covalently closed circular structure and thus lack 3' and 5' ends. Due to this structure, circRNAs are very stable [5, 6], and they are localized and function in the cytoplasm [7].

Previous studies have shown that hsa_circ_0001944 can regulate glycolysis and malignant progression of cancers such as leukemia and gastric cancer [8-10]. The hsa_circ_0001944 is an annotated circular RNA located on chromosome X (chrX:130,883,333-130,928,494, negative strand), with a spliced length of 1096 bp, as recorded in the circBase database. This circRNA has been reported in multiple circRNA sequencing studies and is classified as an internally annotated ncRNA-derived circRNA. However, although hsa_circ_0001944 has been reported to be associated with colorectal cancer progression and prognosis [11], its underlying molecular mechanisms

in CC remain incompletely understood. Therefore, the goals of this study were to identify the biological roles of hsa_circ_0001944 during CC progression and to determine the mechanisms by which it exerts its effects. Overall, our results suggest that hsa_circ_0001944 may be an effective biomarker for CC prognosis and a potential therapy target.

Materials and Methods

Ethics statement

The clinical study was approved and supervised by the Clinical Research Ethics Committee of The First Affiliated Hospital of Anhui Medical University (PJ 2024-01-10). All animal experiments were approved by the Institutional Animal Care and Use Committee of Anhui Medical University (LISC20240365) and were conducted strictly in accordance with institutional guidelines for the care and use of laboratory animals.

Tissue specimens and cell cultures

We obtained both normal tissue and CC tumor samples from The First Affiliated Hospital of Anhui Medical University (China). Human CC cells HT29 (CL-0118), SW480 (CL-0223B), HCT116 (CL-0096), SW837 (CL-0485), SW48 (CL-0513B), RKO (CL-0196) and SW620 (CL-0225B), and normal epithelial cells NCM460 (CL-0749) were obtained from Procell (China). Cells were cultured in Dulbecco's modified Eagle medium (high glucose; 41401ES76, YEASEN, China). The culture medium was supplemented with 10% fetal bovine serum (FBS; 10100139, Thermo Fisher, USA) and 1% penicillin/streptomycin (C0222, Beyotime, China). All cell lines used in this study were authenticated by short tandem repeat profiling and routinely tested negative for mycoplasma contamination prior to experimentation. Fluorescence in situ hybridization (FISH) was performed to determine the subcellular localization of hsa_circ_0001944 in colorectal cancer tissues, adjacent normal tissues, colorectal cancer cell lines, and normal epithelial cells. Quantitative real-time PCR (RT-qPCR) was used to evaluate the expression levels of hsa_circ_0001944 in the same sample sets.

FISH

FISH was performed to determine the subcellular localization of hsa_circ_0001944 in tissues and cell lines. For cell samples, cells were seeded on glass coverslips (84043ES03, YEASEN, China). For tissue samples, paraffin (8002-74-2, NJ-Reagent, China)-embedded sections were deparaffinized, rehydrated through graded ethanol (64-17-5, NJ-Reagent, China), and subjected to antigen retrieval. All samples were fixed with 4% paraformaldehyde (Y261133, Beyotime, China) for 15 min and permeabilized with 0.1% Triton X-100 (20107ES20, YEASEN, China) for 10 min, followed by washing with phosphate-buffered saline (PBS, PB180327, Procell, China). Prehybridization was performed using hybridization buffer (AM8677, Thermo Fisher, USA) at 37°C for 1 h. And samples were subsequently incubated overnight at 37°C with a digoxigenin (Dig)-labeled circ-0001944 probe (5'-GATACTTTATGAGGGACTAAGGTGTCAG-3'; Geneseed Biotech, China). Cell nuclei were counterstained with 4',6-diamidino-2-phenylindole (DAPI, MA0127, MeilunBio, China), and fluorescence images were acquired using a fluorescence microscope (Leica, Germany).

Transfection of cells

SW480 and RKO cells were transfected to investigate the regulatory mechanisms and downstream targets of hsa_circ_0001944. The following transfection constructs were used: short hairpin RNA targeting hsa_circ_0001944 (sh-circ-0001944, forward: 5’-UCUUUAAGAACUCAGUUUCUG-3’; reverse: 5’-GAAACUGAGUUCUUAAAGAGA-3’) and a negative control shRNA (sh-NC, forward: 5’-UUCUUCGAAGGUGUCACGUTT-3’; reverse: 5’-ACGUGACACCUUCGAAGAATT-3’). An IGF2BP1 overexpression plasmid (pcDNA3.1-IGF2BP1) and the corresponding empty vector control (OE-NC) were used for IGF2BP1 gain-of-function experiments. In addition, a miR-665 inhibitor (5'-AGGGGCCUCAGCCUCCUGGU-3'), miR-665 inhibitor negative control (inhibitor-NC) (5'-CAGUACUUUUGUGUAGUACAA-3'), miR-665 mimic (5'-ACCAGGAGGCUGAGGCCCCU-3'), and mimic-NC (5'-

UUCUCCGAACGUGUCACGUTT-3') (GenePharma, China). Cells were transfected using Lipofectamine 3000 (L3000015, Thermo Fisher, USA) according to the manufacturer's instructions. After 48 h of transfection, cells were collected for subsequent experiments. Transfection efficiency was evaluated by quantitative real-time PCR (RT-qPCR). Successfully transfected cells were used for subsequent analyses.

Extracellular acidification rate (ECAR) and oxygen consumption rate (OCR)

SW480 and RKO cells from different treatment groups were seeded in Seahorse XF96 cell culture microplates at a density of 15,000 cells/well and incubated overnight. Seahorse XF Sensor Cartridges (Agilent, USA) were hydrated overnight according to the manufacturer's instructions. Prior to measurement, the culture medium was replaced with Seahorse assay medium (103680-100, Agilent, USA), and cells were incubated in a non-CO_2 incubator for 1 h. For ECAR measurements, glycolytic function was assessed using the Seahorse XF Glycolysis Stress Test. Glucose (10 mM, HY-B0389, MedChemExpress, USA), oligomycin (1 μM, HY-N6782, MedChemExpress, USA), and 2-deoxy-D-glucose (2-DG; 50 mM, HY-13966, MedChemExpress, USA) were sequentially injected during the assay. For OCR measurements, mitochondrial respiration was evaluated using the Seahorse XF Cell Mito Stress Test. Oligomycin (1 μM, HY-N6782, MedChemExpress, USA), carbonyl cyanide-p-trifluoromethoxyphenylhydrazone (FCCP; 1 μM, HY-100410, MedChemExpress, USA), and rotenone (0.5 μM, HY-B1756, MedChemExpress, USA) plus antimycin A (0.5 μM, HY-N12257, MedChemExpress, USA) were sequentially injected during the assay. ECAR and OCR were recorded automatically using the Seahorse XF96 Extracellular Flux Analyzer (Agilent, USA), and data were analyzed using Seahorse Wave software.

RT-qPCR

Total RNA from cells or tumor tissue was extracted using the TRIzol reagent kit (MF0103, Maokangbio, China). For mRNA and circRNA detection, cDNA was synthesized using circRNA RT-qPCR Kit (R0201, Ivdshow, China). For miRNA

detection, reverse transcription was performed using the TaqMan™ MicroRNA Assay Kit (4391848, Thermo Fisher, USA). RT-qPCR was performed using SYBR Green Universal Master Mix (4334973, Thermo Fisher Scientific, USA) for circRNA and mRNA detection, and TaqMan Universal Master Mix II (4440043, Thermo Fisher, USA) for miRNA detection on a Roche real-time PCR system (Roche, USA) under standard cycling conditions. Relative RNA expression levels of hsa_circ_0001944, miR-665, and IGF2BP1 were calculated using the $2^{-\Delta\Delta CT}$ method [12]. *Glyceraldehyde 3-phosphate dehydrogenase(GAPDH)* was used as the internal reference for hsa_circ_0001944 and IGF2BP1, while U6 was used as the internal control for miR-665. Primers utilized were as follows (forward/reverse): hsa_circ_0001944: 5'-TGCAGATACGATGCTGAGTGA-3' / 5'-ACATACTGACACCTTAGTCTCCTC-3'; *miR*-665: 5'-GGTGAACCAGGAGGCTGAGG-3' / 5'-CAGTGCAGGGTCCGAGGTAT-3'; *IGF2BP1*: 5'-CTCCTTTATGCAGGCTCCCG-3' /77 5'-GGGTCTCCAGCTTCACTTCC-3'; *U6*: 5'-CTCGCTTCGGCAGCACATATACTA-3' / 5'-ACGAATTTGCGTGTCATCCTTGCG-3'; *GAPDH*: 5'-TGACTTCAACAGCGACACCCA-3' / 5'-CACCCTGTTGCTGTAGCCAAA-3'.

RNase R Treatment

To verify the circular structure and RNase R resistance of hsa_circ_0001944, total RNA was extracted from SW480 cells and incubated with RNase R (R7092S, Beyotime, China) at 37°C for 10 min to selectively digest linear RNA. An equal amount of untreated RNA was used as the control. Following RNase R treatment, RNA was purified and reverse transcribed into complementary DNA (cDNA) using a reverse transcription kit according to the manufacturer's instructions. RT-qPCR was subsequently performed to detect the expression levels of hsa_circ_0001944 and its corresponding linear transcript.

Cell proliferation

Cell proliferation was assessed using the Cell Counting Kit-8 (CCK-8; 40203ES60,

YEASEN, China). SW480 and RKO cells were seeded into 96-well plates at a density of 5,000 cells per well and cultured overnight. After treatment with the indicated six groups, cell viability was measured at 0, 24, 48, and 72 h. At each time point, 10 μL of CCK-8 reagent was added to each well and incubated for 1 h at 37°C. The absorbance was then measured at 450 nm using a microplate reader (Bio-Rad, US), and cell viability curves were plotted accordingly.

Migration assay

Migration assay was performed using Transwell chambers (FTW076, Beyotime, China). Cells were transfected for 48 h and then resuspended at a density of 2×10^5 cells/mL in serum-free medium. A total of 200 μL of cell suspension was added to the upper chamber, while 500 μL of medium containing 10% FBS was added to the lower chamber as a chemoattractant. After incubation for 24 h, non-migrated cells on the upper surface were gently removed with a cotton swab. Cells that migrated to the lower surface were fixed with methanol and stained with crystal violet. The number of migrated cells was counted under a microscope (Nikon, Japan) in five randomly selected fields per sample.

Dual-luciferase reporter assay

Dual-luciferase reporter assays were performed to validate the interaction between miR-665 and its putative binding sites in IGF2BP1 3'-untranslated region (3'-UTR) and hsa_circ_0001944. The wild-type (WT) and mutant (Mut) sequences were cloned into the psi-CHECK-2 vector (Promega, USA). In this system, Renilla luciferase served as the experimental reporter, while firefly luciferase was used as an internal control to normalize transfection efficiency and cell viability differences. Recombinant plasmids (IGF2BP1-WT/Mut and circ-0001944-WT/Mut) were transfected into SW480 cells using Lipofectamine 3000. After 24-48 h of transfection, luciferase activities were measured using a dual-luciferase reporter assay system (E1910, Promega, USA) according to the manufacturer's instructions.

Ethynyl-2'-deoxyuridine (EdU) assay

Cell proliferation was assessed using an EdU assay kit (CA1176, Solarbio, China). SW480 or RKO cells (1×10^4 cells/well) were seeded into plates and incubated overnight. On the following day, EdU reagent was added, and cells were incubated for 2 h. Cells were then fixed with 4% paraformaldehyde and permeabilized with 0.5% Triton X-100. After washing, cells were stained with Apollo reaction solution according to the manufacturer's instructions. Cell nuclei were counterstained with DAPI. Cell proliferation was visualized and analyzed using a fluorescence microscope.

Western blotting (WB)

Total proteins were extracted from cells using radioimmunoprecipitation (RIPA) lysis buffer (P0013, Beyotime, China) supplemented with protease inhibitors (P1006, Beyotime, China). Protein concentration was determined using a bicinchoninic acid (BCA) protein assay kit (P0009, Beyotime, China). Equal amounts of protein samples were separated by sodium dodecyl sulfate-polyacrylamide gel electrophoresis (SDS-PAGE, P0690, Beyotime, China) and then transferred onto polyvinylidene fluoride (PVDF, FFP24, Beyotime, China) membranes. The membranes were blocked with 5% non-fat milk for 1 h at room temperature and then incubated overnight at 4°C with primary antibodies against pyruvate kinase M2 (PKM2, 15822-1-AP, Proteintech, China, 1:2000), IGF2BP1 (22803-1-AP, Proteintech, China, 1:5000), and β-actin (20536-1-AP, Proteintech, China, 1:4000). The membranes were incubated with HRP-conjugated secondary antibodies (RGAR001, Proteintech, China, 1:3000) for 1 h at room temperature. Protein bands were visualized using an enhanced chemiluminescence (ECL) detection kit (E412, Vazyme, China), and images were captured using a chemiluminescence imaging system (Tanon 5200, China). Band intensities were quantified using ImageJ software.

In vivo experiments

A total of 16 BALB/c nude mice (male, 4-6 weeks old) were purchased from Vitalrive (Beijing, China). To establish the subcutaneous tumor model, SW480 cells transfected

with sh-circ-0001944 or sh-NC (2×10^6 cells in 100 μL PBS) were injected into the flank of nude mice (n = 5 per group). Tumor volume was measured every 5 days. Thirty days after cell inoculation, mice were anesthetized with 4% isoflurane (R510-22-10, RWD, China, inhalation anesthesia) and euthanized by cervical dislocation. Tumors were then excised and weighed. For the metastasis model, SW480 cells stably expressing firefly luciferase were injected via the tail vein (n = 3 per group). Four weeks after injection, mice were anesthetized with 4% isoflurane and euthanized by cervical dislocation. Lung tissues were collected for analysis. Metastatic nodules were evaluated using bioluminescence imaging and confirmed by histological examination. Animals were monitored daily for general health status, body weight, and behavior throughout the experiment. Humane endpoints were established before the study. Mice showing severe distress, impaired mobility, persistent inability to access food or water, body weight loss exceeding 20%, or signs of moribundity were immediately euthanized to minimize suffering. All animals reached the planned experimental endpoint, and no unexpected deaths occurred during the study. Death was confirmed by the absence of respiration and heartbeat, loss of corneal reflex, and fixed, dilated pupils following cervical dislocation.

Immunohistochemistry

Paraffin-embedded tumor tissues were sectioned into 5 μm-thick slices. Antigen retrieval was performed using citrate buffer (C2488, Sigma-Aldrich, USA). Sections were blocked with 5% bovine serum albumin (BSA; ST025, Beyotime, China) at room temperature for 1 h, followed by incubation with the primary antibody against Ki67 (ab16667, Abcam, UK) at 4°C overnight. After washing with PBS, sections were incubated with the corresponding secondary antibody (ab205718, Abcam, UK) for 1 h at room temperature. Immunoreactivity was visualized using a 3,3'-diaminobenzidine (DAB) substrate kit (ab64238, Abcam, UK). Sections were then counterstained with hematoxylin (H9627, Sigma-Aldrich, USA), and images were observed under a light microscope.

Statistical analyses

All experiments were independently repeated at least three times. Data are denoted by means ± standard deviation (SD). All data were analyzed using GraphPad Prism (GraphPad, USA). Comparisons between two groups were performed using an unpaired Student's t-test, while comparisons among multiple groups were analyzed using one-way analysis of variance (ANOVA) followed by Tukey's post hoc test. $P < 0.05$ was considered to be significantly different.

Results

Hsa_circ_0001944 expression was higher in CC tissues and cell lines compared to normal cells and tissues

Accumulating evidence has shown that circular RNAs (circRNAs) play important roles in regulating the tumor microenvironment and malignant progression of CC [13, 14]. In addition, previous studies have reported that hsa_circ_0001944 contributes to glycolysis and tumor growth in colorectal cancer [8-10]. In the current study, FISH analysis showed that hsa_circ_0001944 expression was significantly higher in cancer tissues compared to corresponding normal tissue (Fig. 1A). Additionally, hsa_circ_0001944 was mainly distributed in the cytoplasm of cells (Fig. 1A). RT-qPCR data showed that hsa_circ_0001944 expression was higher in CC tissue compared to normal tissue (Fig. 1B) and that hsa_circ_0001944 expression was higher in HT29, SW480, HCT116, SW837, SW48, RKO, and SW620 cells compared to NCM460 cells, particularly in SW480 and RKO (Fig. 1C). FISH outputs demonstrated that hsa_circ_0001944 was mainly distributed in the cytoplasm in SW480 and RKO cells (Fig. 1D). We also confirmed that hsa_circ_0001944 was not affected by RNase R (Fig. 1E). Bioinformatics analyses illustrated that hsa_circ_0001944 was generated by cyclizing 15 exons from the *Maass2017* gene located on chrX:130883333-130928494 (Fig. 1F).

Hsa_circ_0001944 silencing inhibited CC proliferation and cell growth capability

RT-qPCR data illustrated that hsa_circ_0001944 expression was downregulated in

SW480 and RKO cells after hsa_circ_0001944 silencing via sh-circ-0001944 treatment (Fig. 2A). CCK-8 results showed that hsa_circ_0001944 downregulation inhibited the proliferation ability of both SW480 and RKO cells (Fig. 2B, C), and EdU outcomes showed the same result (Fig. 2D–F). Tumor formation in xenografts of nude mice using SW480 cells showed that hsa_circ_0001944 silencing significantly reduced tumor growth ability (Fig. 2G–I). Immunohistochemistry with Ki67 staining verified that hsa_circ_0001944 silencing suppressed Ki67 expression in tumor tissues (Fig. 2J–K). These results indicated that hsa_circ_0001944 downregulation suppressed CC cell proliferation and tumor growth.

Downregulation of hsa_circ_0001944 suppressed CC cell migration and pulmonary metastasis

Transwell migration assay data showed that hsa_circ_0001944 silencing suppressed CC cell migration in SW480 and RKO cells (Fig. 3A, B). Live imaging data verified that luc-SW480 cells exhibited pulmonary metastasis but that hsa_circ_0001944 silencing reduced the pulmonary metastasis capability (Fig. 3C–F). These findings showed that hsa_circ_0001944 downregulation suppressed CC cell migration and pulmonary metastasis.

miR-665 and IGF2BP1 are downstream targets of hsa_circ_0001944

Bioinformatics analysis showed that miR-665 and miR-2278 are downstream targets of hsa_circ_0001944 (Fig. 4A). Luciferase reporter assay data confirmed that miR-665 inhibited luciferase activity in wild-type (Wt) but not in mutated (Mut) cell lines (Fig. 4B), indicating that miR-665 is an hsa_circ_0001944 target. The luciferase reporter data also showed that miR-665 can interact with the 3'-UTR of IGF2BP1 (Fig. 4C, D).

RT-qPCR data showed that hsa_circ_0001944 expression decreased after its downregulation (Fig. 4E, F). In contrast, miR-665 inhibition did not affect hsa_circ_0001944 expression (Fig. 4E, F), indicating that miR-665 is a downstream target of hsa_circ_0001944. Additionally, silencing hsa_circ_0001944 significantly increased miR-665 expression, suggesting that hsa_circ_0001944 functions as a sponge

for miR-665 (Fig. 4G, H). Conversely, inhibition of miR-665 reversed the effects of hsa_circ_0001944 knockdown on miR-665 expression (Fig. 4G, H). Hsa_circ_0001944 silencing also reduced IGF2BP1 expression (Fig. 4I, J). Transfection with a miR-665 inhibitor or overexpression of IGF2BP1 significantly increased IGF2BP1 expression (Fig. 4I, J), suggesting that miR-665 and IGF2BP1 are downstream targets of hsa_circ_0001944.

Overexpression of IGF2BP1 or inhibition of miR-665 restored CC proliferation and migration ability after hsa_circ_0001944 silencing

EdU data (Fig. 5A–D) and Transwell migration assay results (Fig. 5E–H) showed that IGF2BP1 overexpression or miR-665 inhibition restored cell proliferation ability and migration ability, respectively, after silencing of hsa_circ_0001944 in SW480 and RKO cells. These findings suggest that hsa_circ_0001944 expression enhances CC progression by regulating the miR-665/IGF2BP1 axis.

Overexpression of IGF2BP1 restored CC proliferation and migration ability after expression of miR-665

RT-qPCR data showed that miR-665 overexpression promoted miR-665 expression and that miR-665 mimic treatment inhibited IGF2BP1 expression (Fig. 6A–D). Overexpression of IGF2BP1 restored and promoted IGF2BP1 expression but did not influence miR-665 expression (Fig. 6A–D). EdU data (Fig. 6E–H) and Transwell migration assay results (Fig. 6I–L) showed that overexpression of IGF2BP1 restored CC cell proliferation ability and migration ability, respectively, after overexpression of miR-665 in both SW480 and RKO cells. These results suggest that miR-665 expression inhibits CC progression by regulating the miR-665/IGF2BP1 axis.

Overexpression of IGF2BP1 restored aerobic glycolysis of CC after silencing of hsa_circ_0001944

WB analysis showed that silencing of hsa_circ_0001944 inhibited both IGF2BP1 and PKM2 expression. However, overexpression of IGF2BP1 promoted both IGF2BP1 and

PKM2 expression after sh-circ-0001944 treatment (Fig. 7A, B).

Seahorse XFe96 Analyzer assessment of the bioenergetic profiles of SW480 and RKO cells revealed that the ECAR values of the glycolytic proton efflux rate in both cell types treated with sh-circ-0001944 adjuvant were significantly lower than those of the NC, but that inhibition of miR-665 reversed the suppressive effects of sh-circ-0001944 on the glycolytic ability of CC cells (Fig. 7C, D). The basal OCR values, as well as ATP production and maximal respiration values, were significantly higher in the sh-circ-0001944 groups compared to the NC, but inhibition of miR-665 reversed the promotive effect of sh-circ-0001944 on mitochondrial respiration in CC cells and facilitated the oxidative phosphorylation process (Fig. 7E, F).

Discussion

Previous studies have reported that circRNAs play an important role in regulating the malignant progression of CC [4, 6]. Various pathological factors are involved in the tumor progression of CC, and circRNA can regulate a series of tumor phenotypes, including metastasis, chemotherapy resistance, and aerobic glycolysis [15]. The results of the current study showed that hsa_circ_0001944 expression was higher in CC tissues and cells than in normal controls. We also found that silencing hsa_circ_0001944 with sh-circ-0001944 inhibited the proliferation, migration, tumor growth, and pulmonary metastasis of CC cells. Together with previous reports that circ-0001944 drives aerobic glycolysis and malignant progression in cancers [8, 10, 16], our findings suggest that hsa_circ_0001944 functions importantly in the progression of CC.

Bioinformatics and luciferase reporter assay outcomes verified that miR-665 and IGF2BP1 are downstream targets of hsa_circ_0001944. Previous studies showed that miR-665 is expressed abnormally in cancers in multiple systems, including neural, respiratory, and digestive systems [17], and that miR-665 expression suppresses the progression of cancers, including bladder cancer, osteosarcoma, breast cancer, and gastric cancer [18-21]. Our results showed that silencing of hsa_circ_0001944 increased miR-665 expression and that miR-665 overexpression reversed the inhibitory effects of sh-circ-0001944 on the proliferation and migration ability of CC cells. These

results show that overexpression of miR-665 inhibits CC cell proliferation and migration.

We also confirmed that IGF2BP1 is a downstream target of miR-665. Previous studies have shown that IGF2BP1 is an RNA-binding protein that regulates cellular proliferation and invasion [22, 23] and that it is a potent N6-methyladenosine reader protein in cancer [24]. It also enhances tumor progression in various solid tumors, which is associated with adverse prognosis [25]. Our results showed that hsa_circ_0001944 downregulation decreased IGF2BP1 expression but that IGF2BP1 overexpression reversed the inhibitory effects of sh-circ-0001944 or miR-665 on CC cell proliferation and migration abilities.

Aerobic glycolysis is an indispensable mechanism in tumorigenesis and development [26], and PKM2 is a key enzyme in the last step of glycolysis. Our seahorse extracellular flux analysis revealed that hsa_circ_0001944 downregulation inhibited aerobic glycolysis and that overexpression of IGF2BP1 reversed aerobic glycolysis after silencing of hsa_circ_0001944. Lv et al. previously showed that IGF2BP1 can interact with PKM2 and promote aerobic glycolysis [27]. We also found that downregulation of hsa_circ_0001944 inhibited both IGF2BP1 and PKM2 expression and that overexpression of IGF2BP1 increased PKM2 expression. These results suggest that hsa_circ_0001944 can regulate aerobic glycolysis of CC by influencing miR-665/IGF2BP1/PKM2.

This study has several limitations. First, although hsa_circ_0001944 was significantly upregulated in colorectal cancer tissues and cells, the clinical sample size was limited, and larger independent cohorts are needed to validate its clinical relevance. Second, the interactions among hsa_circ_0001944, miR-665, and IGF2BP1 were primarily validated using bioinformatic prediction and dual-luciferase reporter assays. Additional approaches, such as RNA immunoprecipitation and RNA pull-down assays, are required to further confirm these direct molecular interactions. Third, while the present study demonstrated that hsa_circ_0001944 regulates glycolysis through the miR-665/IGF2BP1/PKM2 axis, other downstream signaling pathways and metabolic alterations remain to be investigated.

Taken together, our results revealed that oncogenic hsa_circ_0001944 is upregulated in CC tissues and cells and that high hsa_circ_0001944 expression is correlated with high CC cell aggression. Hsa_circ_0001944 can promote the malignant progression of CC by modulating the miR-665/IGF2BP1/PKM2 axis. This study provides a potential candidate for CC treatment.

Abbreviations

CC	**Colorectal cancer**
FISH	**Fluorescence in situ hybridization**
RT-qPCR	**real-time quantitative PCR**
CCK-8	**Cell Counting Kit-8**
EdU	**ethynyl-2'-deoxyuridine**
ECAR	**extracellular acidification rate**
OCR	**oxygen consumption rate**
IGF2BP1	**2 mRNA-binding protein 1**
PKM2	**pyruvate kinase M2**
ncRNAs	**non-coding RNAs**
circRNAs	**Circular RNAs**
GAPDH	**Glyceraldehyde 3-phosphate dehydrogenase**
cDNA	**complementary DNA**
WT	**wild-type**
Mut	**mutant**
WB	**Western blotting**
SD	**standard deviation**
ANOVA	**analysis of variance**

Ethics approval and consent to participate

The Ethics Committee of The First Affiliated Hospital of Anhui Medical University approved and supervised this investigation, including all animal experiments. (LLSC20240365)

Consent for publication

All participants have given their consent for the publication of this manuscript.

Availability of data and materials

All data generated or analysed during this study are included in this published article and its supplementary information files.

Competing interests

The authors declare no competing interests.

Funding:

None.

Authors' Contribution

Conception and design of the research: Ruhang Zhou, Xudong Jiang and Jun Lei

Acquisition of data: Xiaosi Hu, Aman Xu

Analysis and interpretation of data: Ruhang Zhou, Xudong Jiang, Aman Xu and Jun Lei

Statistical analysis: Xiaosi Hu, Aman Xu

Drafting the manuscript: Zhaibiao Wang, Xiaosi Hu and Aman Xu

Revision of manuscript for important intellectual content: Ruhang Zhou, Zhaibiao Wang

Acknowledgements

None.

References

1. Abedizadeh, R., et al., *Colorectal cancer: a comprehensive review of carcinogenesis, diagnosis, and novel strategies for classified treatments.* Cancer Metastasis Rev, 2024. **43**(2): p. 729-753.
2. Patel, S.G., et al., *The rising tide of early-onset colorectal cancer: a comprehensive review of epidemiology, clinical features, biology, risk factors, prevention, and early detection.* Lancet Gastroenterol Hepatol, 2022. **7**(3): p. 262-274.
3. *Global, regional, and national burden of colorectal cancer and its risk factors, 1990-2019: a systematic analysis for the Global Burden of Disease Study 2019.* Lancet Gastroenterol Hepatol, 2022. **7**(7): p. 627-647.
4. Zhang, Y., et al., *CircRNAs in colorectal cancer: potential biomarkers and therapeutic targets.* Cell Death & Disease, 2023. **14**(6): p. 353.
5. Memczak, S., et al., *Circular RNAs are a large class of animal RNAs with regulatory potency.* Nature, 2013. **495**(7441): p. 333-8.
6. Xu, H., et al., *CircRNA_0000392 promotes colorectal cancer progression through the miR-193a-5p/PIK3R3/AKT axis.* J Exp Clin Cancer Res, 2020. **39**(1): p. 283.
7. Kristensen, L.S., et al., *The biogenesis, biology and characterization of circular RNAs.* Nat Rev Genet, 2019. **20**(11): p. 675-691.
8. Dou, Y., et al., *Circ_0001944 Contributes to Glycolysis and Tumor Growth by Upregulating NFAT5 Through Acting as a Decoy for miR-142-5p in Non-Small Cell Lung Cancer.* Cancer Manag Res, 2021. **13**: p. 3775-3787.
9. Zhong, B., et al., *Hsa_circ_0001944 regulates apoptosis by regulating the binding of PARP1 and HuR in leukemia and malignant transformed cells induced by hydroquinone.* Environ Toxicol, 2023. **38**(2): p. 381-391.
10. Liu, R., et al., *Hsa_circ_0001944 enhanced GSPT1 expression via sponging miR-498 to promote proliferation and invasion of gastric cancer.* J Clin Lab Anal, 2023. **37**(2): p. e24810.
11. Duan, H. and J. Qiu, *Association of has_circ_0001944 upregulations with prognosis and cancer progression in patients with colorectal cancer.* Discov Oncol, 2022. **13**(1): p. 23.
12. Fiedler, S.D., M.Z. Carletti, and L.K. Christenson, *Quantitative RT-PCR methods for mature microRNA expression analysis*, in *RT-PCR Protocols: Second Edition*. 2010, Springer. p. 49-64.
13. Shang, A., et al., *Exosomal circPACRGL promotes progression of colorectal cancer via the miR-142-3p/miR-506-3p- TGF-β1 axis.* Mol Cancer, 2020. **19**(1): p. 117.
14. Yao, B., et al., *CircEZH2/miR-133b/IGF2BP2 aggravates colorectal cancer progression via enhancing the stability of m(6)A-modified CREB1 mRNA.* Mol Cancer, 2022. **21**(1): p. 140.
15. Wang, X., et al., *Exosome-delivered circRNA promotes glycolysis to induce chemoresistance through the miR-122-PKM2 axis in colorectal cancer.* Mol Oncol, 2020. **14**(3): p. 539-555.
16. Fu, B., et al., *Circular RNA circBCBM1 promotes breast cancer brain metastasis by modulating miR-125a/BRD4 axis.* Int J Biol Sci, 2021. **17**(12): p. 3104-3117.
17. Guan, X., et al., *Hsa-miR-665 Is a Promising Biomarker in Cancer Prognosis.* Cancers (Basel), 2023. **15**(20).
18. Wang, W., et al., *miR-665 inhibits epithelial-to-mesenchymal transition in bladder cancer via the SMAD3/SNAIL axis.* Cell Cycle, 2021. **20**(13): p. 1242-1252.

19. Zhang, B., et al., *Exosomes loaded with miR-665 inhibit the progression of osteosarcoma in vivo and in vitro.* Am J Transl Res, 2022. **14**(10): p. 7012-7026.
20. Xu, H., et al., *circAR-E2E4-miR-665-STAT3 axis is a potential regulatory network in triple-negative breast cancer.* Heliyon, 2023. **9**(1): p. e12654.
21. Wu, K.Z., et al., *miR-665 Suppresses the Epithelial-Mesenchymal Transition and Progression of Gastric Cancer by Targeting CRIM1.* Cancer Manag Res, 2020. **12**: p. 3489-3501.
22. Huang, X., et al., *Insulin-like growth factor 2 mRNA-binding protein 1 (IGF2BP1) in cancer.* J Hematol Oncol, 2018. **11**(1): p. 88.
23. Zhang, L., et al., *IGF2BP1 overexpression stabilizes PEG10 mRNA in an m6A-dependent manner and promotes endometrial cancer progression.* Theranostics, 2021. **11**(3): p. 1100-1114.
24. Müller, S., et al., *The oncofetal RNA-binding protein IGF2BP1 is a druggable, post-transcriptional super-enhancer of E2F-driven gene expression in cancer.* Nucleic Acids Res, 2020. **48**(15): p. 8576-8590.
25. Glaß, M., et al., *IGF2BP1, a Conserved Regulator of RNA Turnover in Cancer.* Front Mol Biosci, 2021. **8**: p. 632219.
26. Bose, S., C. Zhang, and A. Le, *Glucose Metabolism in Cancer: The Warburg Effect and Beyond.* Adv Exp Med Biol, 2021. **1311**: p. 3-15.
27. Lv, J., et al., *HNRNPL induced circFAM13B increased bladder cancer immunotherapy sensitivity via inhibiting glycolysis through IGF2BP1/PKM2 pathway.* J Exp Clin Cancer Res, 2023. **42**(1): p. 41.

Patient consent for publication

Not application

Use of artificial intelligence tools

During the preparation of this work, AI tool (ChatGPT) was used to improve the readability and language of the manuscript, and subsequently, the authors revised and edited the content produced by the AI tools as necessary, taking full responsibility for the ultimate content of the present manuscript.

Data availability

Figure legends

Figure 1. Hsa_circ_0001944 expression was higher in both CC tissues and cell lines relative to healthy cells.

(A) Fluorescence in situ hybridization (FISH) analysis showing the expression and subcellular localization of hsa_circ_0001944 in CC tissues and adjacent normal tissues. (B) RT-qPCR analysis of hsa_circ_0001944 expression in CC tissues and adjacent normal tissues. Data are presented as mean ± SD from three independent experiments. Statistical significance was analyzed using Student's t-test. ***P < 0.001 vs. normal tissues. (C) RT-qPCR analysis of hsa_circ_0001944 expression in NCM460 cells and CC cell lines (HT29, SW480, HCT116, SW837, SW48, RKO, and SW620). Data are presented as mean ± SD from three independent experiments. Statistical significance was analyzed using one-way ANOVA followed by Tukey's post hoc test. **P < 0.01, ***P < 0.001 vs. NCM460. (D) FISH analysis showing the subcellular localization of hsa_circ_0001944 in SW480 and RKO cells. Representative images are shown. Cell nuclei were counterstained with DAPI (blue). (E) RT-qPCR analysis of linear Maass2017 transcript and circular hsa_circ_0001944 expression following RNase R treatment. Total RNA was treated with or without RNase R prior to reverse transcription. Data are presented as mean ± SD from three independent experiments. Statistical significance was analyzed using Student's t-test. ***P < 0.001 vs. NC. (F) Schematic illustration of the genomic locus and back-splicing formation of hsa_circ_0001944 derived from the Maass2017 gene. The black arrow indicates the back-splicing junction site responsible for circular RNA formation.

Figure 2.Silencing hsa_circ_0001944 suppresses colorectal cancer cell

proliferation in vitro and tumor growth in vivo.

(A) RT-qPCR analysis of hsa_circ_0001944 expression in SW480 and RKO cells following transfection with sh-circ-0001944 or NC. Data are presented as mean ± SD from three independent experiments. Statistical significance was analyzed using Student's t-test. ***P < 0.001 vs. NC. (B and C) CCK-8 assays showing the proliferation of SW480 and RKO cells after hsa_circ_0001944 knockdown. Data are presented as mean ± SD from three independent experiments performed in triplicate. Statistical significance was analyzed using two-way ANOVA. ***P < 0.001 vs. NC. (D-F) EdU incorporation assays showing the proliferative activity of SW480 and RKO cells following hsa_circ_0001944 silencing. EdU-positive nuclei are shown in green. Quantitative results are presented as mean ± SD from three independent experiments. Statistical significance was analyzed using Student's t-test. ***P < 0.001 vs. NC. (G) Representative images of subcutaneous tumors excised from nude mice injected with SW480 cells transfected with NC or sh-circ-0001944. (H) Tumor growth curves showing tumor volumes measured every 5 days after inoculation. Five mice were included in each group (n = 5). Data are presented as mean ± SD. Statistical significance was analyzed using repeated-measures ANOVA. ***P < 0.001 vs. NC. (I) Tumor weights were measured 30 days after cell inoculation. Five mice were included in each group (n = 5). Data are presented as mean ± SD. Statistical significance was analyzed using Student's t-test. ***P < 0.001 vs. NC. (J) Quantitative analysis of Ki67-positive cells in xenograft tumor tissues. Data are presented as mean ± SD (n = 5 mice per group). Statistical significance was analyzed using Student's t-test. ***P < 0.001 vs. NC. (K) Representative immunohistochemical staining images showing Ki67 expression in xenograft tumor tissues.

Figure 3. Silencing hsa_circ_0001944 inhibits colorectal cancer cell migration and pulmonary metastasis.

(A, B) Transwell migration assays showing the migratory abilities of SW480 and RKO cells following hsa_circ_0001944 knockdown. Quantitative data are presented as mean ± SD from three independent experiments. Statistical significance was analyzed using

Student's t-test. ***P < 0.001 vs. NC. (C) Representative bioluminescence imaging of nude mice injected with luciferase-expressing SW480 cells transfected with sh-NC or sh-circ-0001944. Three mice were included in each group. (D) Quantification of pulmonary metastatic burden based on bioluminescence intensity. Data are presented as mean ± SD (n = 3 mice per group). Statistical significance was analyzed using Student's t-test. ***P < 0.001 vs. NC.

(E) Representative hematoxylin and eosin (H&E)-stained lung tissue sections showing metastatic lesions. (F) Quantitative analysis of metastatic foci in lung tissues based on H&E staining. Data are presented as mean ± SD (n = 3 mice per group). Statistical significance was analyzed using Student's t-test. ***P < 0.001 vs. NC.

Figure 4. hsa_circ_0001944 regulates miR-665 and IGF2BP1 expression in colorectal cancer cells.

(A) Schematic illustration of the predicted binding sites between hsa_circ_0001944 and miR-665. The corresponding mutant (Mut) hsa_circ_0001944 sequence containing mutations within the miR-665 binding region is shown. (B) Dual-luciferase reporter assay in SW480 cells co-transfected with hsa_circ_0001944-Wt or hsa_circ_0001944-Mut reporter plasmids and miR-665 mimic or NC mimic. Relative luciferase activity was normalized to Renilla luciferase activity. Data are presented as mean ± SD from three independent experiments. Statistical significance was analyzed using Student's t-test. ***P < 0.001. (C) Schematic illustration of the predicted miR-665 binding site within the IGF2BP1 3'-UTR. The corresponding mutant (Mut) IGF2BP1 3'-UTR sequence is shown. (D) Dual-luciferase reporter assay in SW480 cells co-transfected with IGF2BP1 3'-UTR-Wt or IGF2BP1 3'-UTR-Mut reporter plasmids and miR-665 mimic or NC mimic. Relative luciferase activity was normalized to Renilla luciferase activity. Data are presented as mean ± SD from three independent experiments. Statistical significance was analyzed using Student's t-test. ***P < 0.001. (E-J) RT-qPCR analysis of hsa_circ_0001944, miR-665 and IGF2BP1 expression in SW480 and RKO cells following transfection with sh-circ-00019444, miR-665 inhibitor or IGF2BP1 overexpression. Data are presented as mean ± SD from three independent

experiments. Statistical significance was analyzed using one-way ANOVA followed by Tukey's post hoc test. **P < 0.01, ***P < 0.001 vs. NC; ###P < 0.001 vs. sh-circ-0001944.

Figure 5. miR-665 inhibition or IGF2BP1 overexpression reverses the suppressive effects of hsa_circ_0001944 knockdown on colorectal cancer cell proliferation and migration.

(A-D) EdU incorporation assays showing the proliferative activity of SW480 and RKO cells following hsa_circ_0001944 knockdown, miR-665 inhibitor transfection, or IGF2BP1 overexpression. EdU-positive nuclei are shown in green, and total nuclei were counterstained with DAPI (blue). Quantitative data are presented as mean ± SD from three independent experiments. Statistical significance was analyzed using one-way ANOVA followed by Tukey's post hoc test. *P < 0.05, **P < 0.01, ***P < 0.001 vs. NC; ###P < 0.001 vs. sh-circ-0001944. (E-H) Transwell migration assays showing the migratory abilities of SW480 and RKO cells following hsa_circ_0001944 knockdown, miR-665 inhibitor transfection, or IGF2BP1 overexpression. Quantitative data are presented as mean ± SD from three independent experiments. Statistical significance was analyzed using one-way ANOVA followed by Tukey's post hoc test. *P < 0.05, **P < 0.01, ***P < 0.001 vs. NC; ###P < 0.001 vs. sh-circ-0001944.

Figure 6. IGF2BP1 overexpression reverses the inhibitory effects of miR-665 overexpression on colorectal cancer cell proliferation and migration.

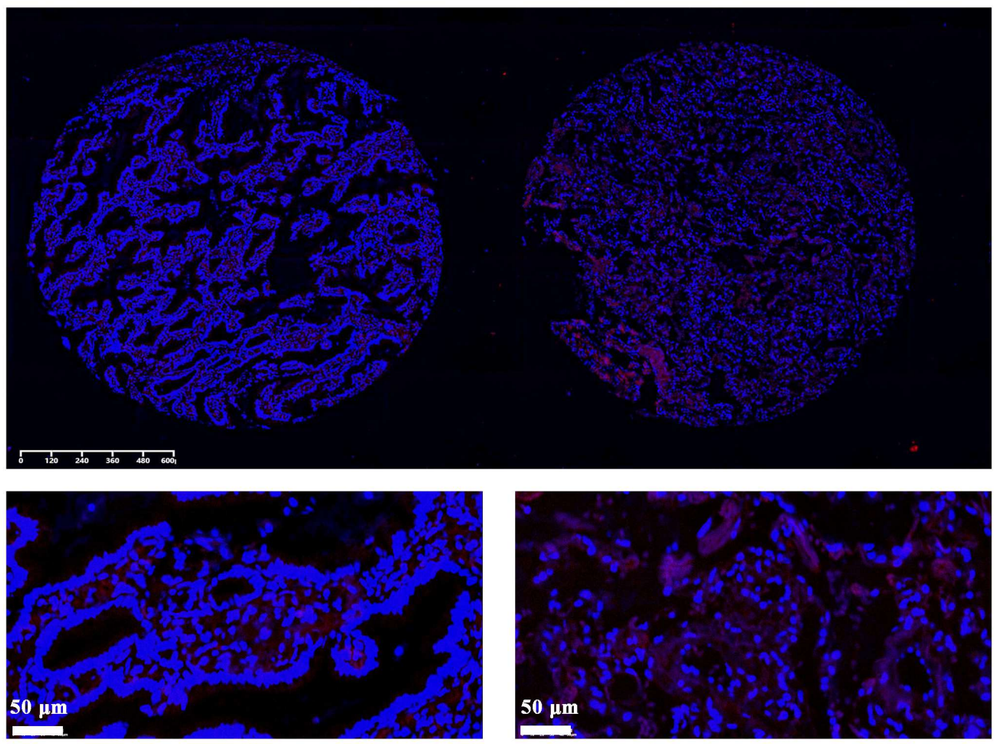
(A-D) RT-qPCR analysis of miR-665 and IGF2BP1 expression in SW480 and RKO cells following transfection with miR-665 mimic and/or IGF2BP1 overexpression plasmid. Data are presented as mean ± SD from three independent experiments. Statistical significance was analyzed using one-way ANOVA followed by Tukey's post hoc test. **P < 0.01, ***P < 0.001 vs. NC; ###P < 0.001 vs. miR-665 mimic. (E-H) EdU incorporation assays showing the proliferative activity of SW480 and RKO cells following miR-665 mimic transfection and/or IGF2BP1 overexpression. EdU-positive nuclei are shown in green, and total nuclei were counterstained with DAPI (blue).

Quantitative data are presented as mean ± SD from three independent experiments. Statistical significance was analyzed using one-way ANOVA followed by Tukey's post hoc test. *P < 0.05, **P < 0.01, ***P < 0.001 vs. NC; ##P < 0.01 vs. miR-665 mimic. (I-L) Transwell migration assays showing the migratory abilities of SW480 and RKO cells following miR-665 mimic transfection and/or IGF2BP1 overexpression. Quantitative data are presented as mean ± SD from three independent experiments. Statistical significance was analyzed using one-way ANOVA followed by Tukey's post hoc test. *P < 0.05, ***P < 0.001 vs. NC; ##P < 0.01, ###P < 0.001 vs. miR-665 mimic.

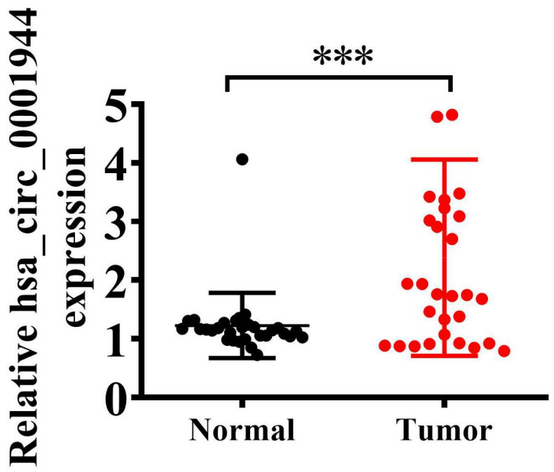
Figure 7. IGF2BP1 overexpression restores aerobic glycolysis following hsa_circ_0001944 knockdown in colorectal cancer cells.

(A-B) Western blot analysed IGF2BP1 and PKM2 protein expression in SW480 and RKO cells following hsa_circ_0001944 knockdown and/or IGF2BP1 overexpression. GAPDH was used as the loading control. Data are presented as mean ± SD from three independent experiments. Statistical significance was analyzed using one-way ANOVA followed by Tukey's post hoc test. ***P < 0.001 vs. NC. (C-F) Seahorse extracellular flux analyses were performed to evaluate cellular metabolic activity in SW480 and RKO cells. The extracellular acidification rate (ECAR) and oxygen consumption rate (OCR) were measured using a Seahorse XF96 Extracellular Flux Analyzer.

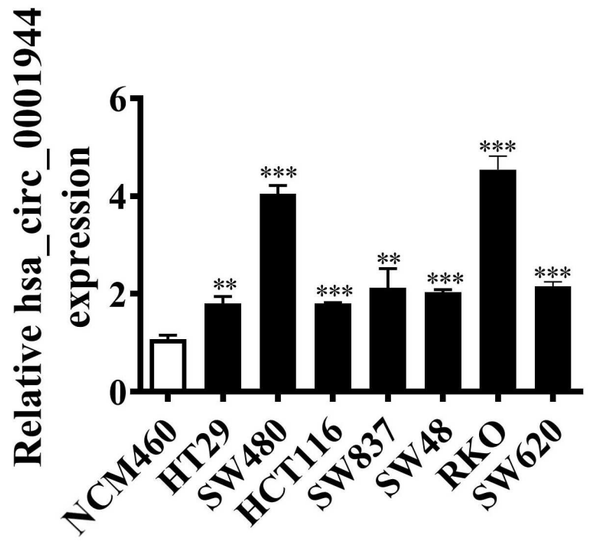
A


Normal
Cancer
50 μm
50 μm

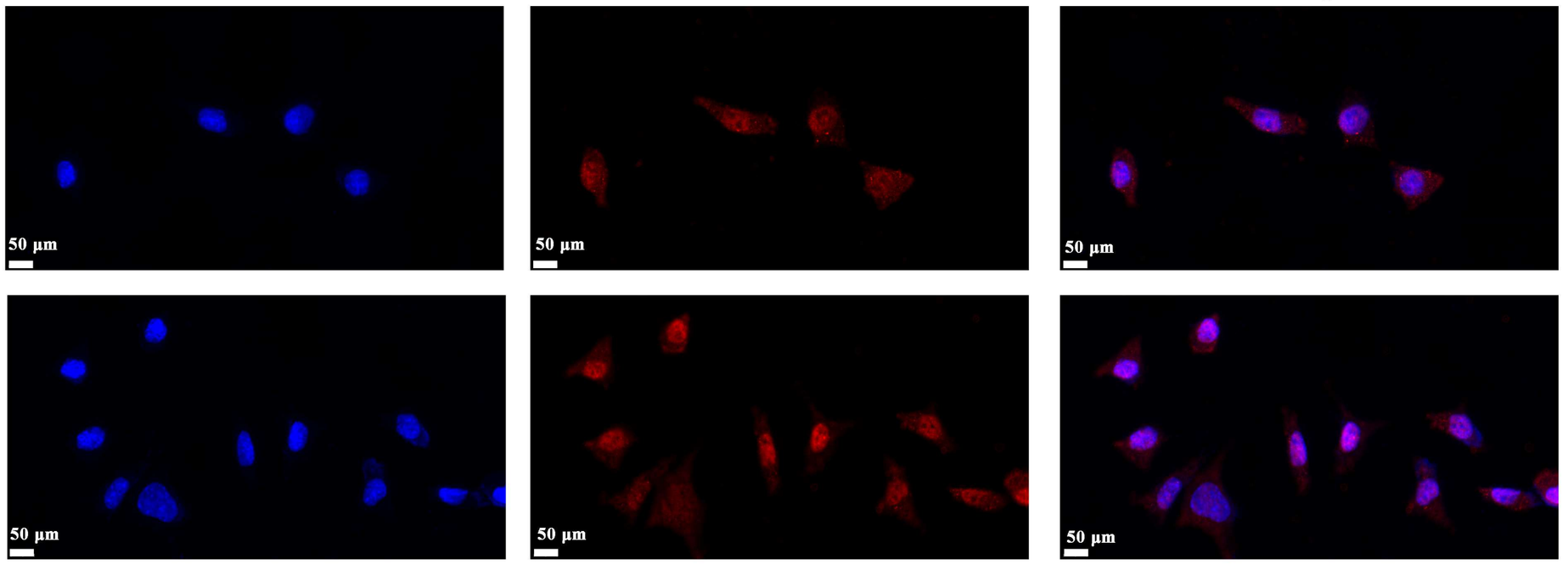
B


***
Relative hsa_circ_0001944 expression
Normal
Tumor

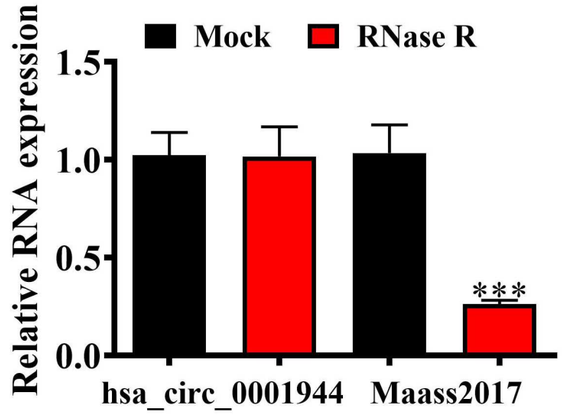
C


Relative hsa_circ_0001944 expression
NCM460
HT29
SW480
HCT116
SW837
SW48
RKO
SW620

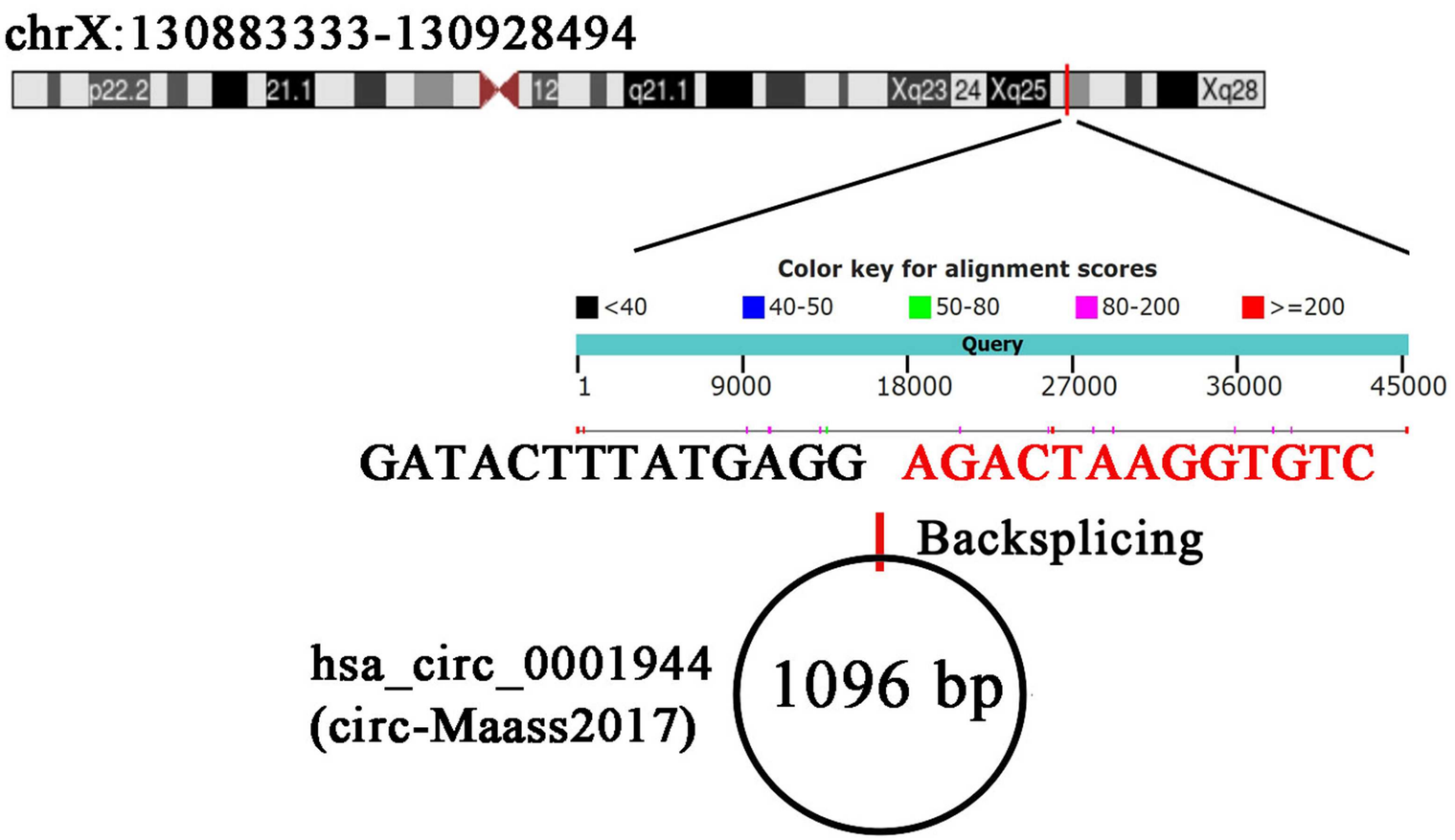
D


DAPI
hsa_circ_0001944
Merge
SW480
RKO
50 μm

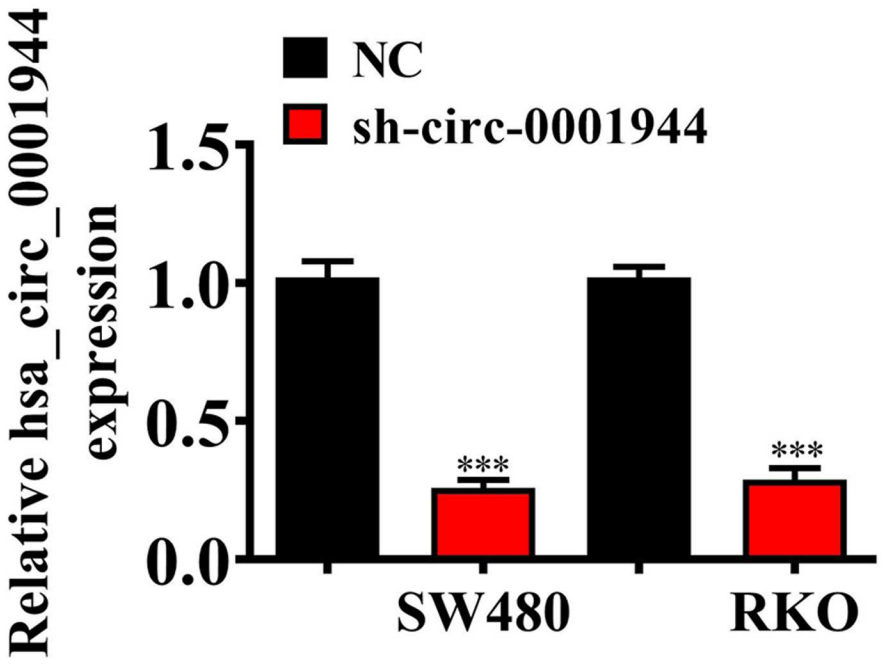
E


Mock
RNase R
Relative RNA expression
***
hsa_circ_0001944
Maass2017

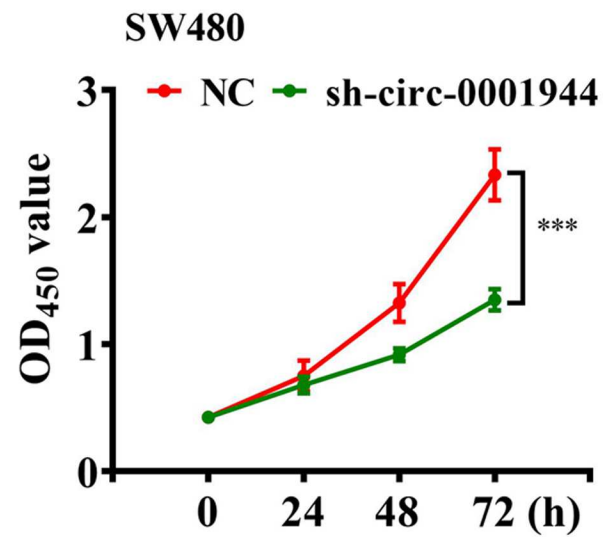
F


chrX:130883333-130928494
p22.2
21.1
12
q21.1
Xq23
24
Xq25
Xq28
Color key for alignment scores
<40
40-50
50-80
80-200
>=200
Query
1
9000
18000
27000
36000
45000
GATACTTTATGAGG AGACTAAGGTGTC
Backsplicing
hsa_circ_0001944
(circ-Maass2017)
1096 bp

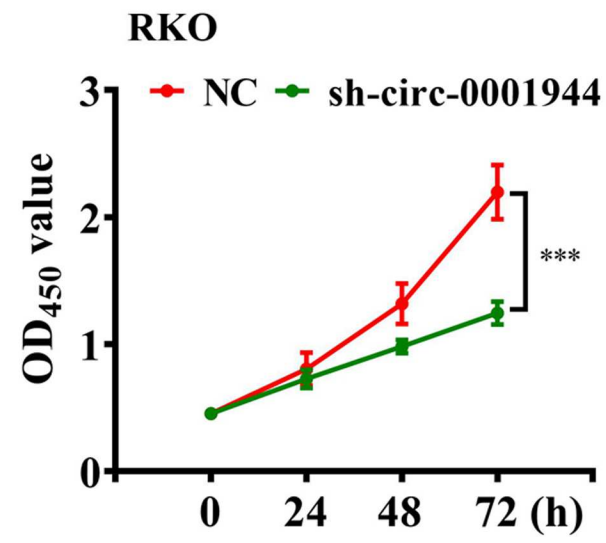
A



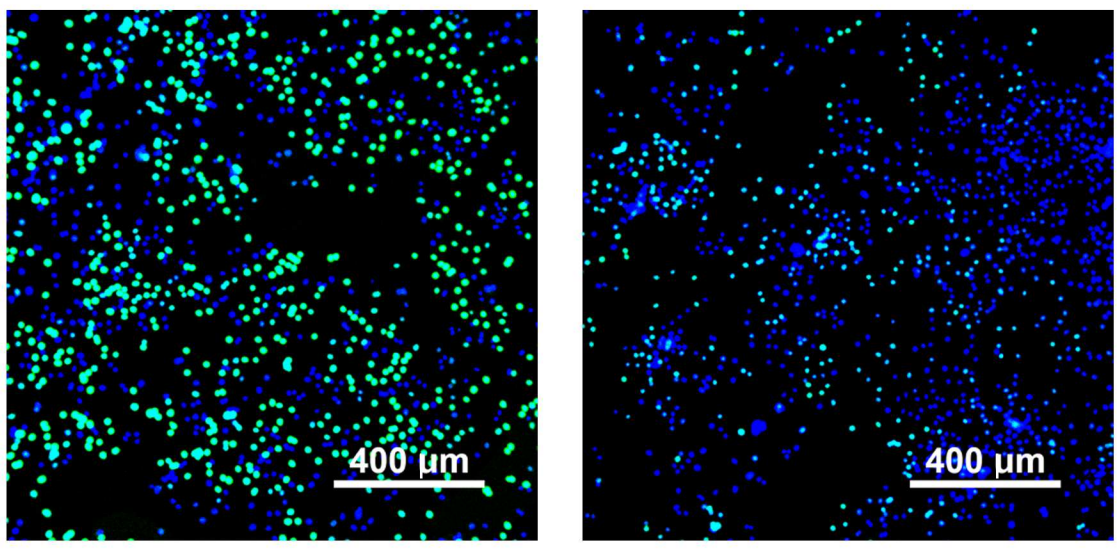
B



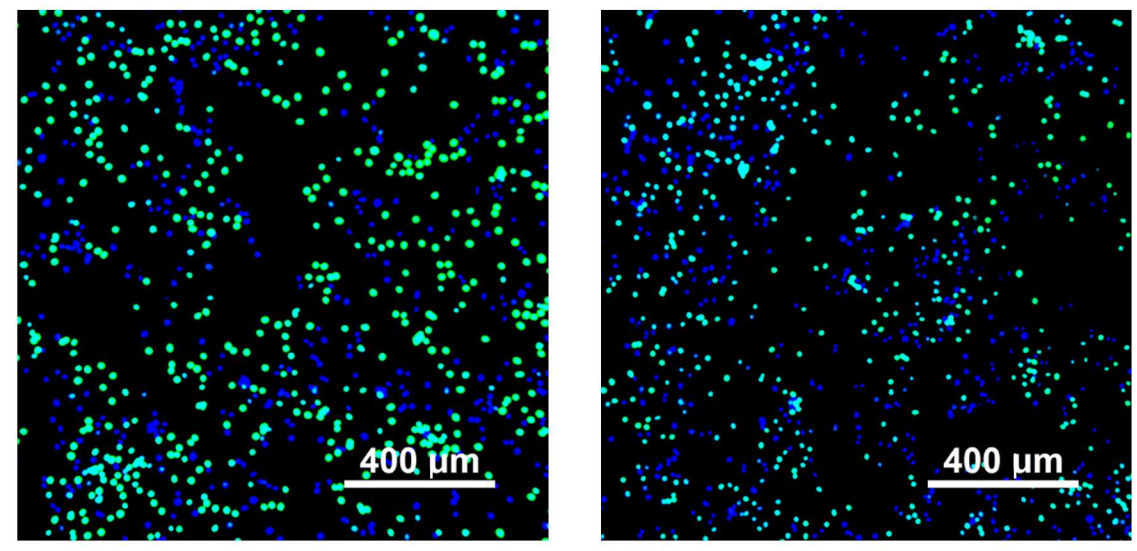
C



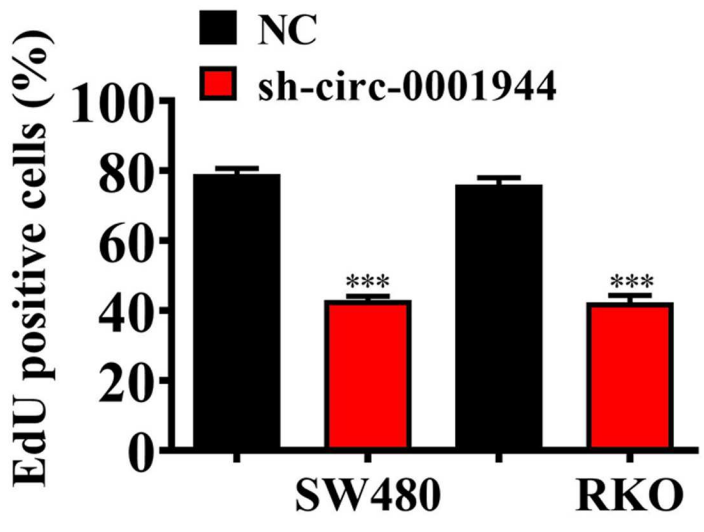
D



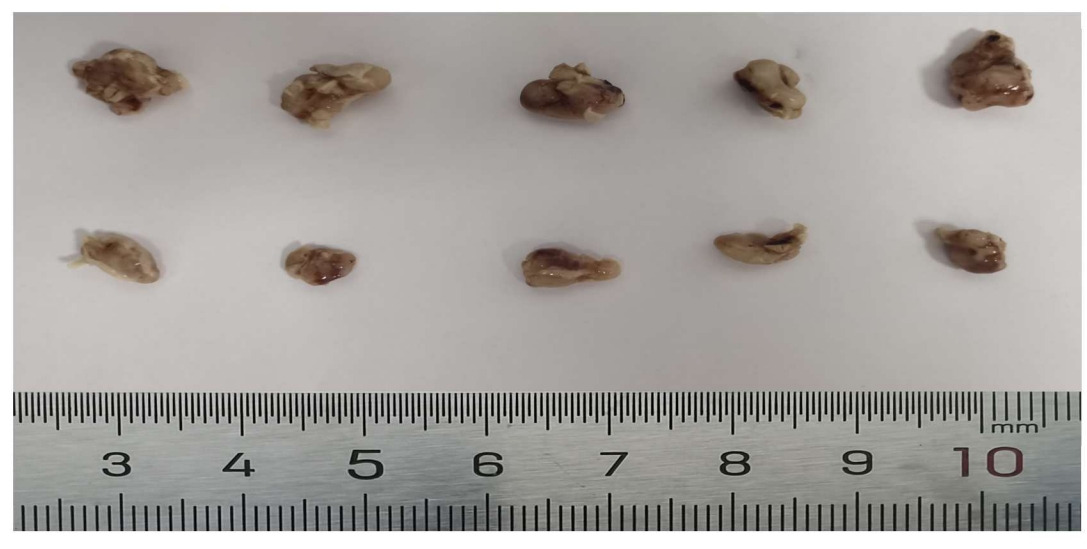
E



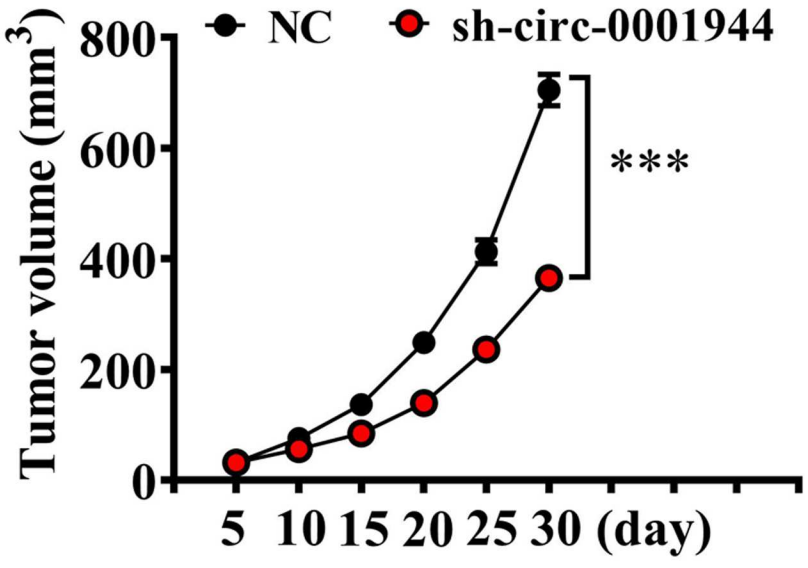
F



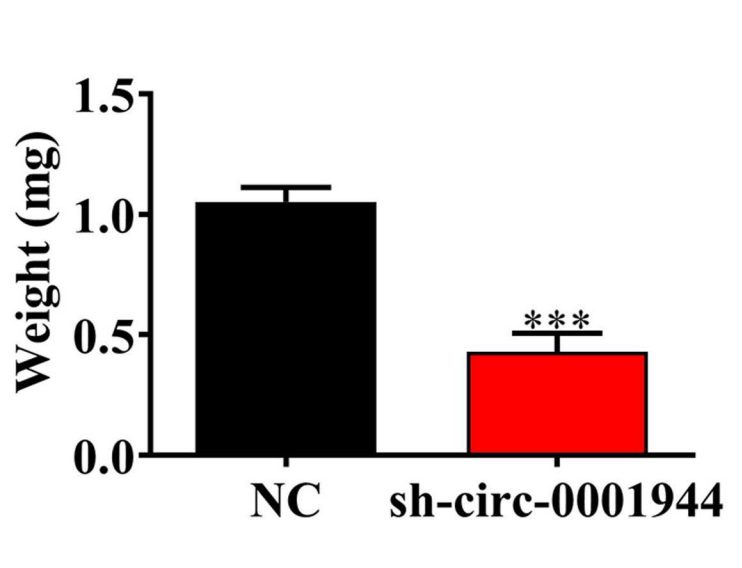
G



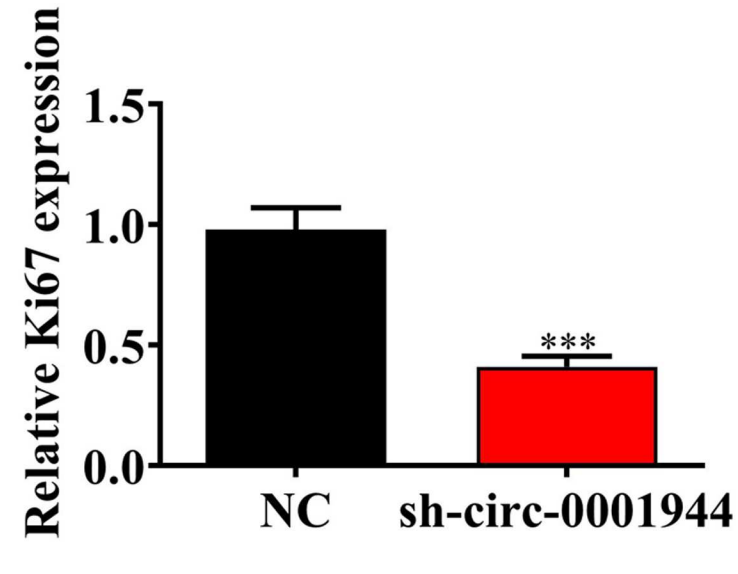
H



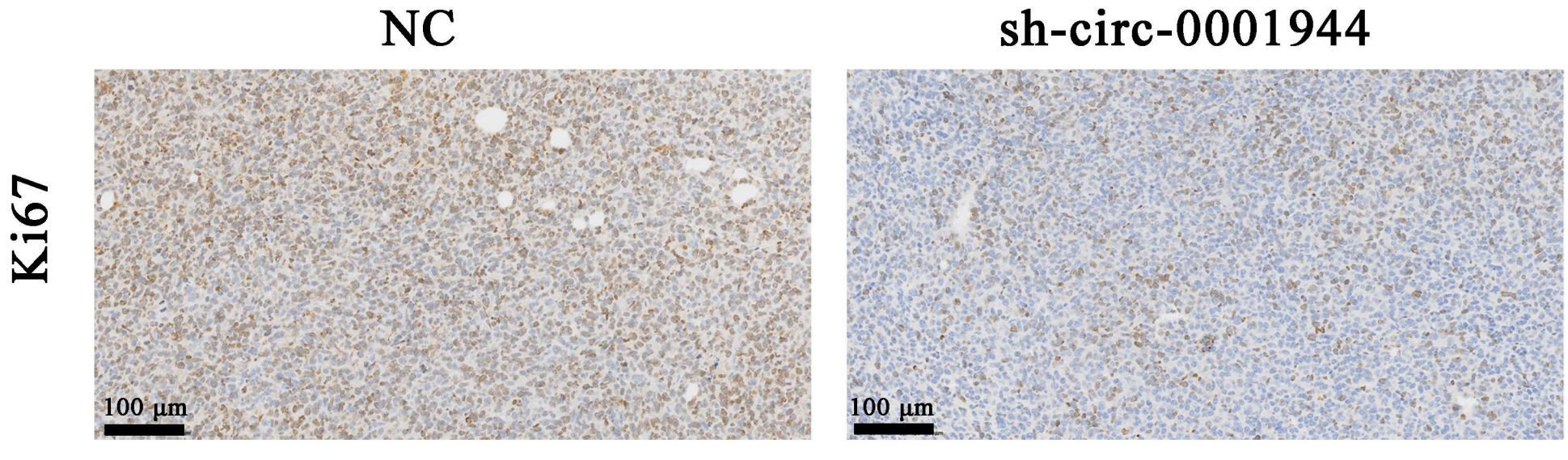
I

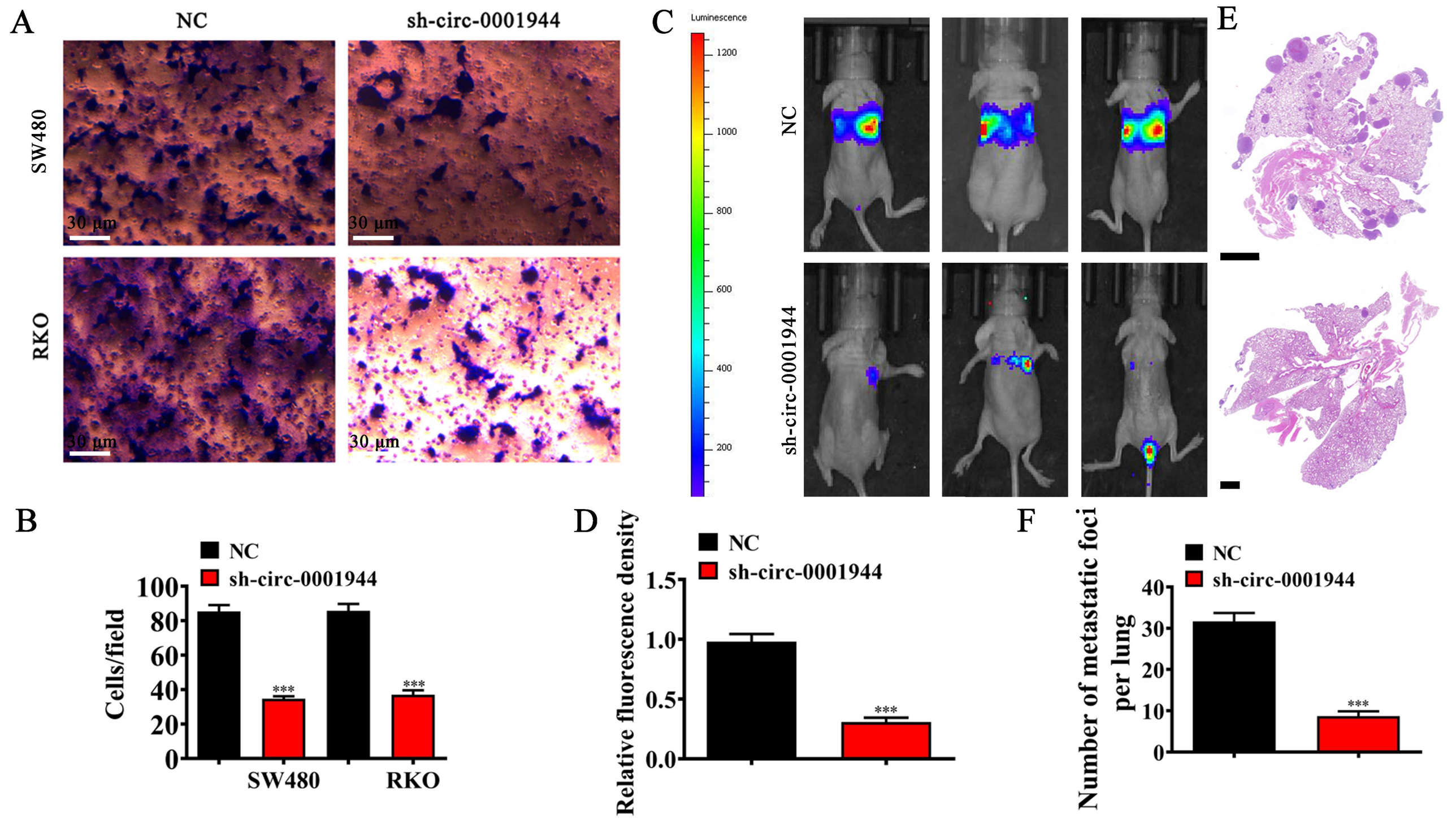


J



K




A
NC
sh-circ-0001944
SW480
RKO
30 μm
30 μm
30 μm
30 μm
C
Luminescence
1200
1000
800
600
400
200
NC
sh-circ-0001944
E
B
NC
sh-circ-0001944
Cells/field
100
80
60
40
20
0
***
***
SW480
RKO
D
NC
sh-circ-0001944
Relative fluorescence density
1.5
1.0
0.5
0.0
***
F
NC
sh-circ-0001944
Number of metastatic foci per lung
40
30
20
10
0
***

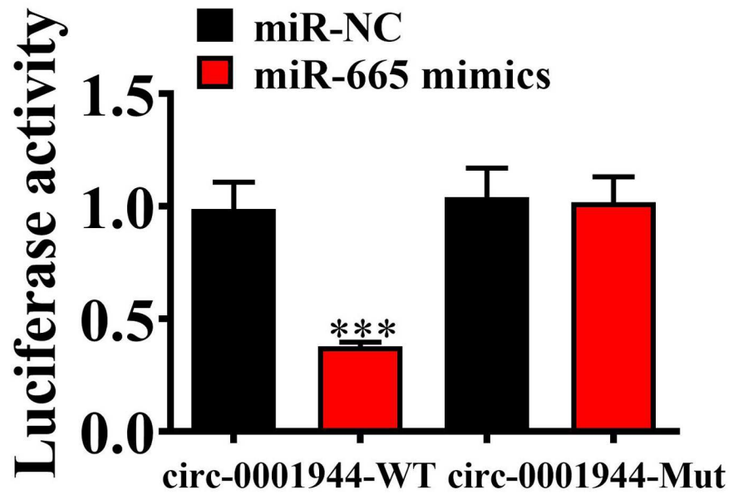
A

hsa_circ_001992-WT: 5' AAGCUGCUCUG--CUCCUGGG 3'

miR-665: 3' UCCCCGGAGUCGGAGGACCA 5'

hsa_circ_001992-Mut: 5' AAGCUGCUCUG--CUGGACCG 3'

B



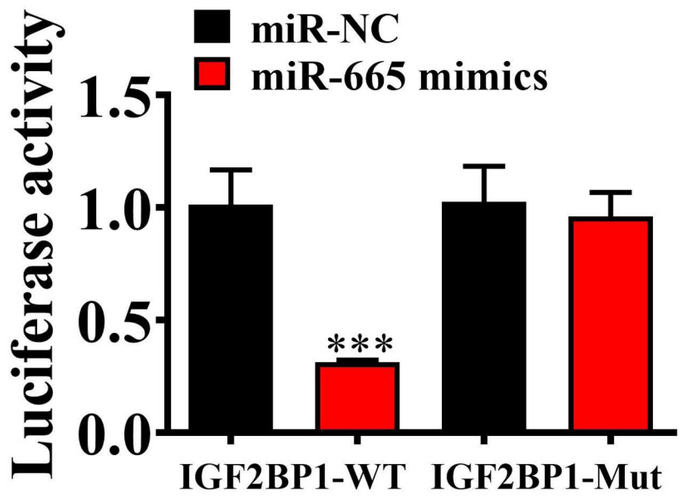
C

IGF2BP1-3'-UTR-WT: 5' UCCAGGAUCUUGAUCCUGGU 3'

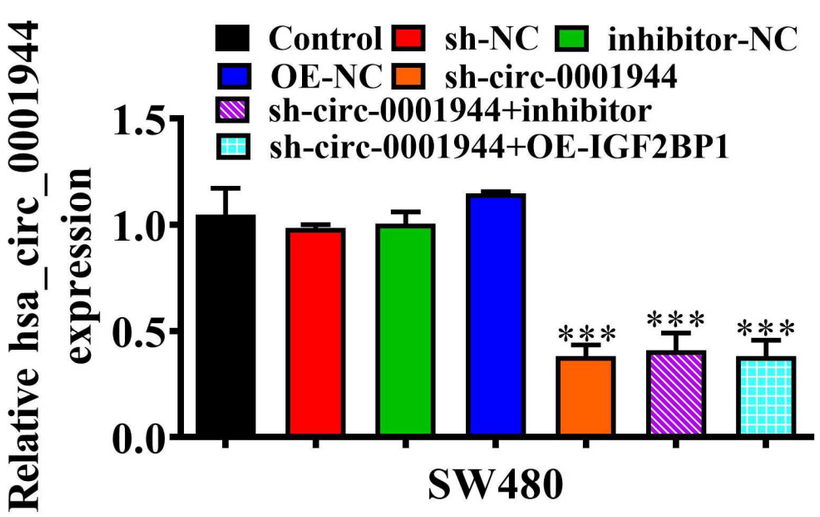
miR-665: 3' UCCCCGGAGUCGGAGGACCA 5'

IGF2BP1-3'-UTR-Mut: 5' UCCAGGAUCUUGAUGGACCU 3'

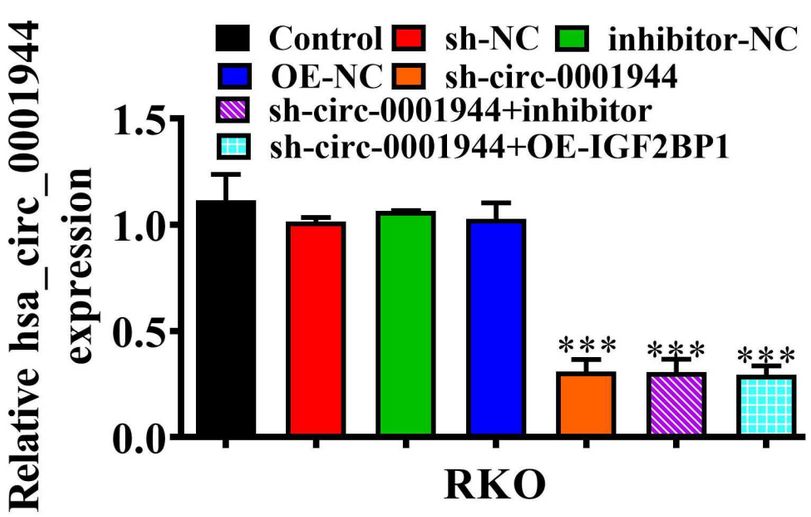
D



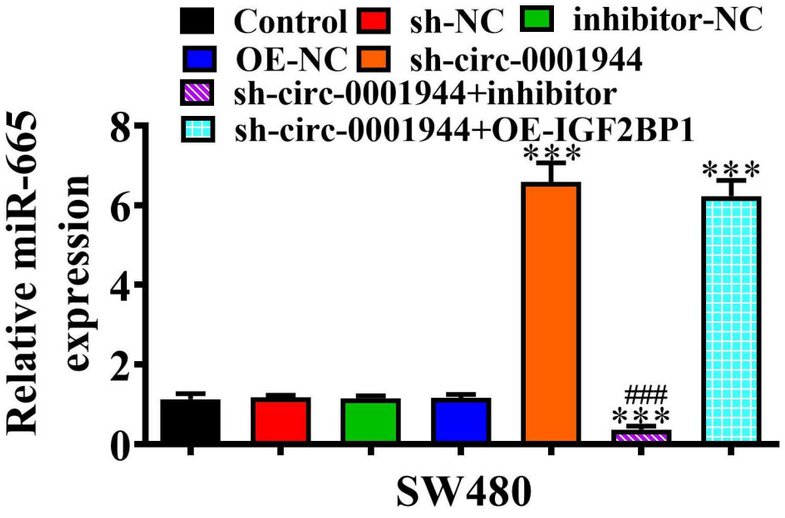
E



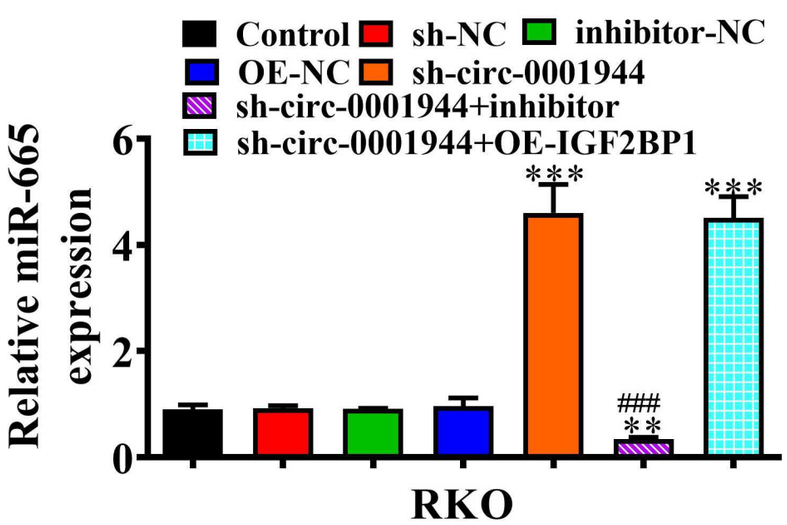
F



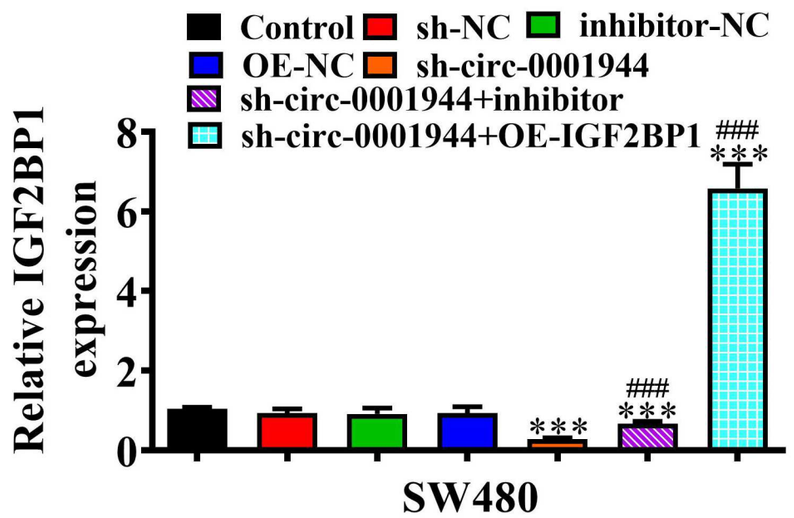
G



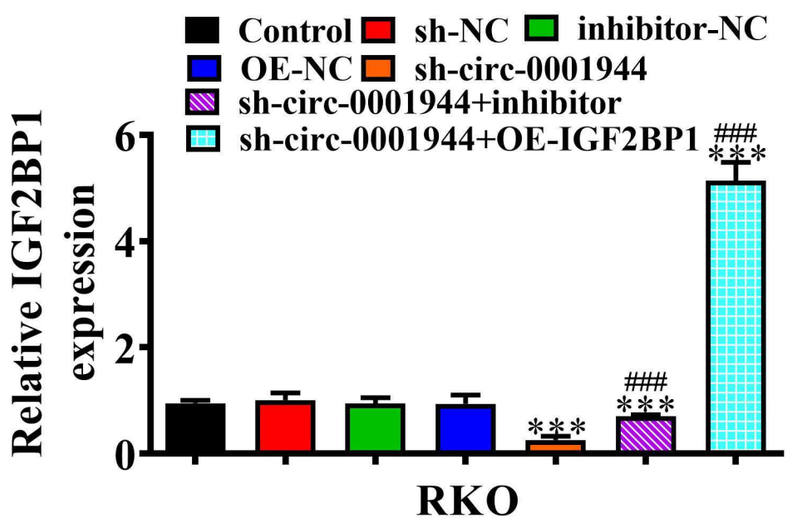
H



I



J



A

NC

sh-circ-0001944

sh-circ-0001944 +miR-665 inhibitor

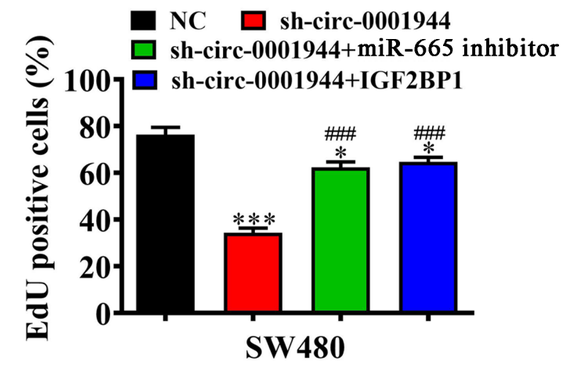
sh-circ-0001944 +IGF2BP1

SW480

RKO

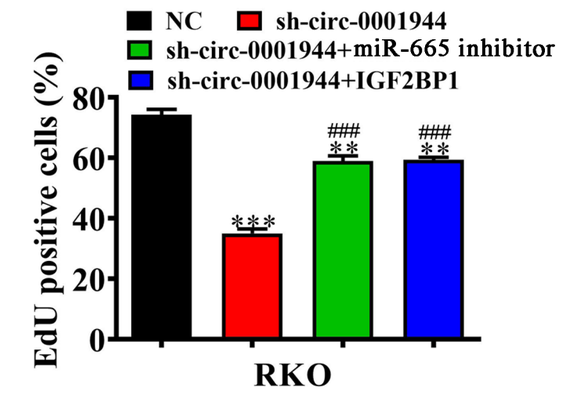
400 μm

B



C

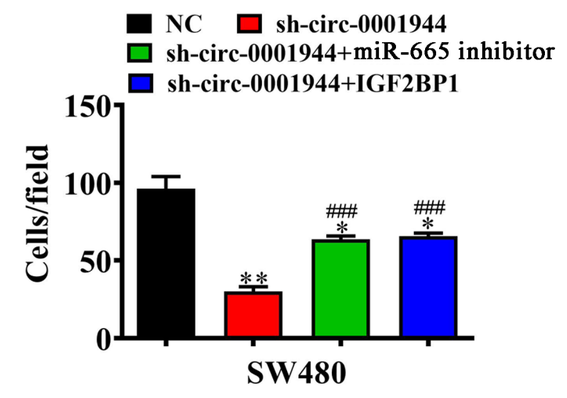
D



E

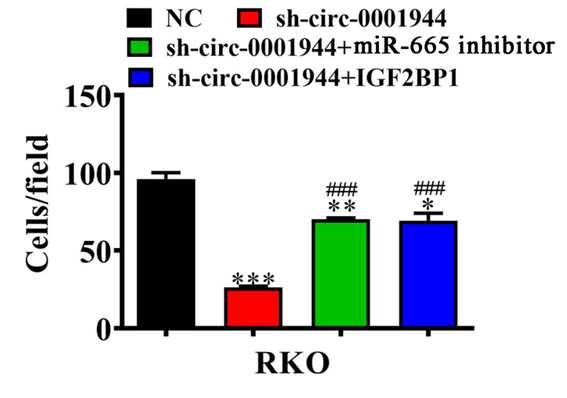
50 μm

F

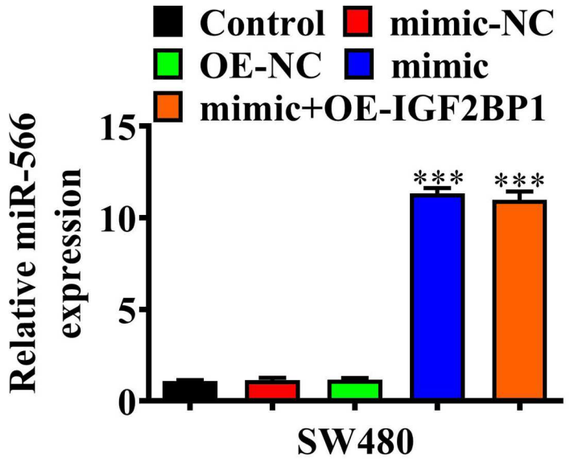


G

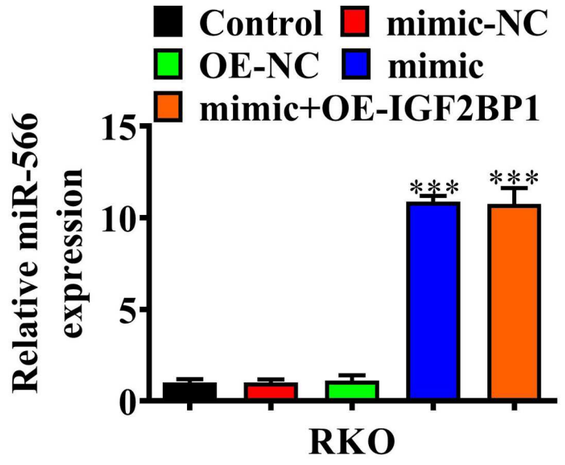
H



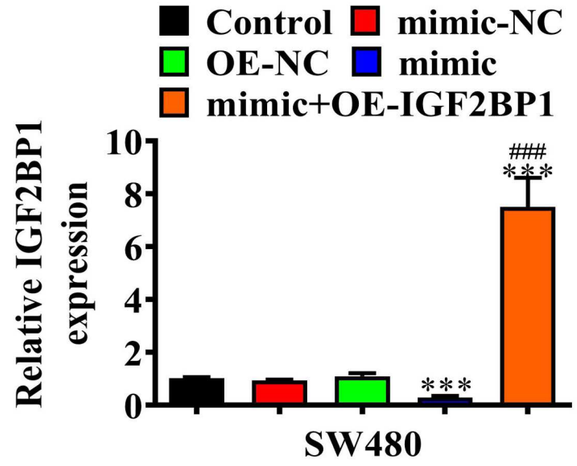
A



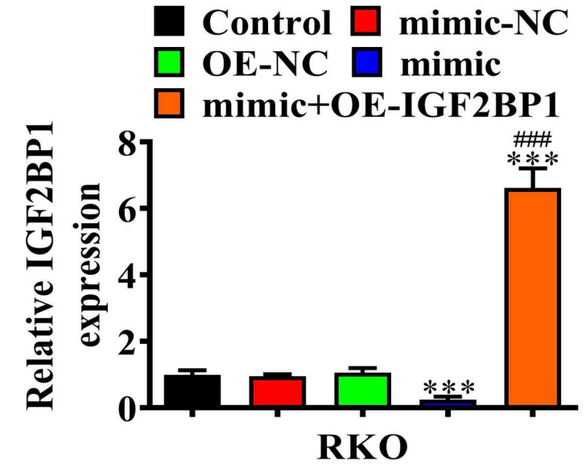
B



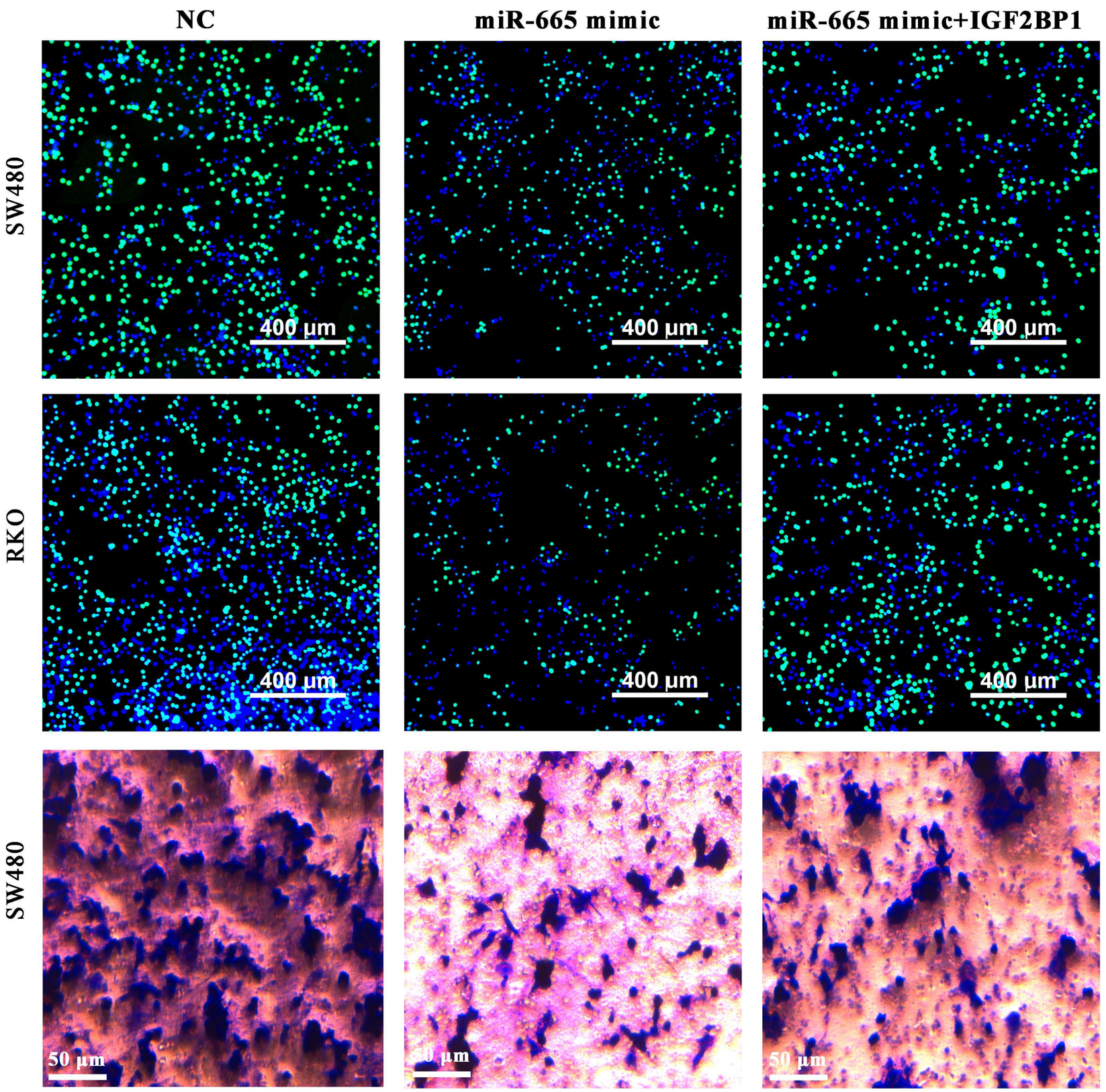
C



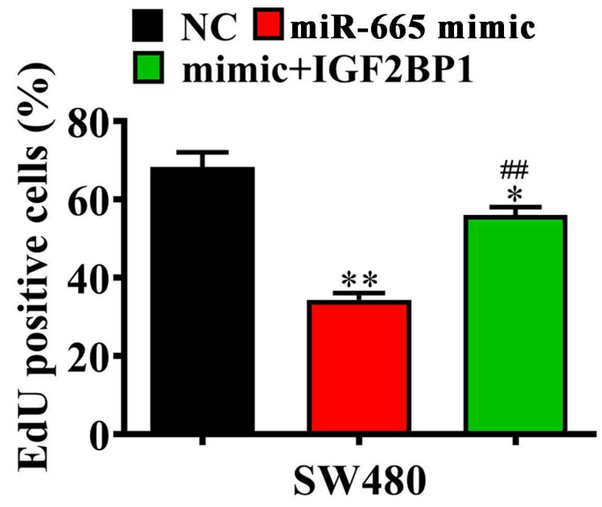
D



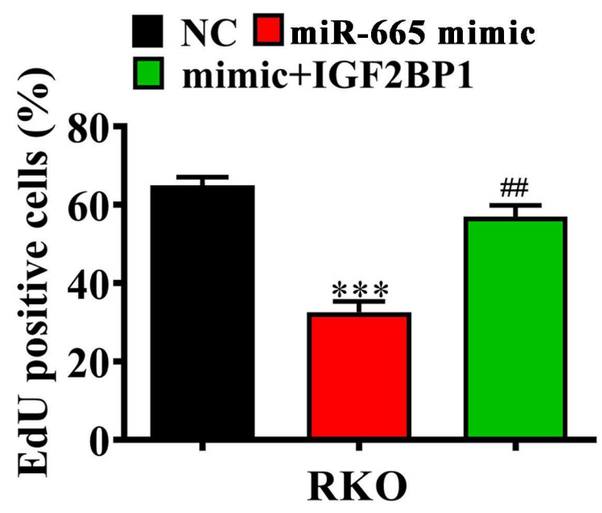
E



F

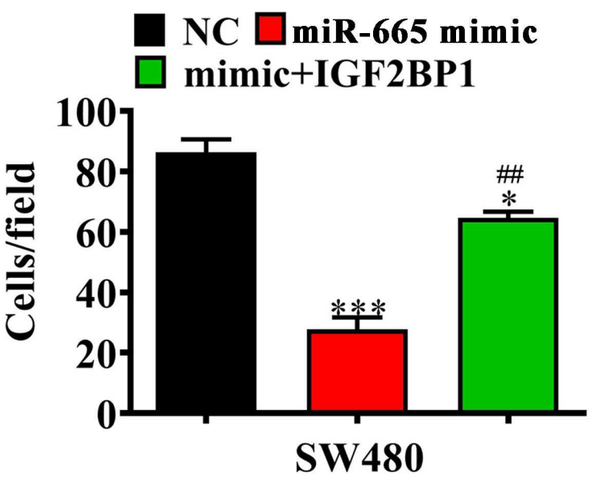


H



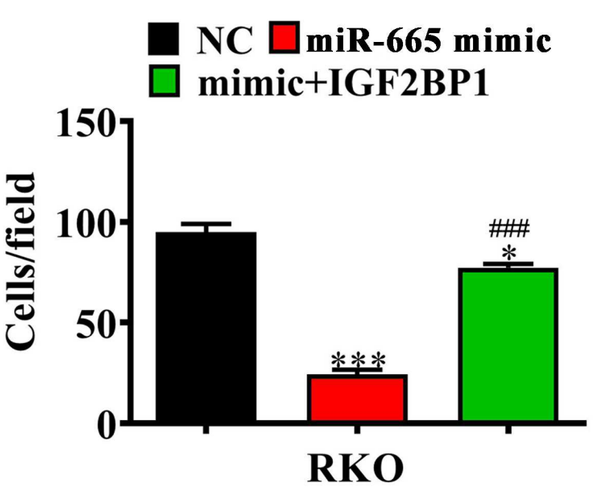
I

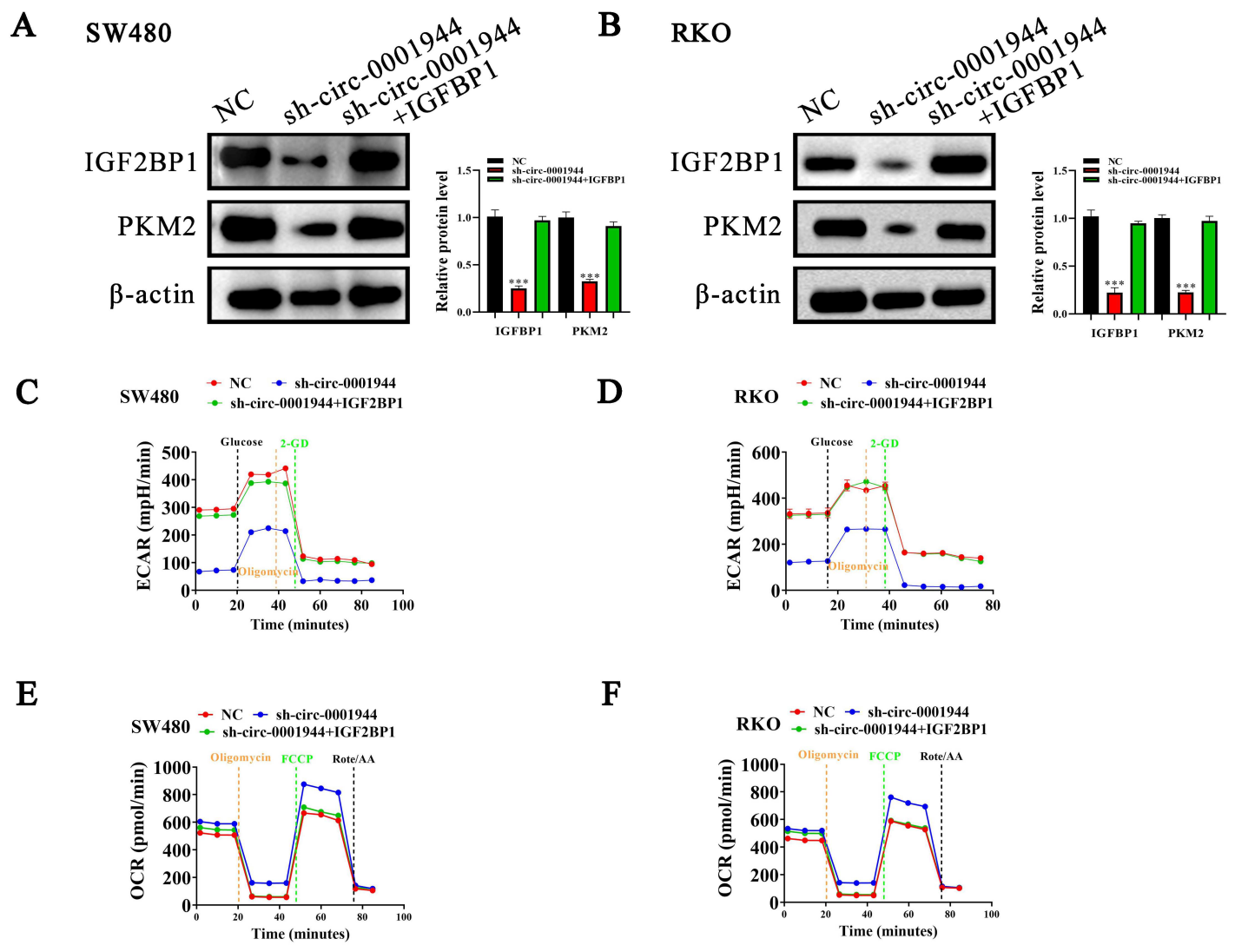
J



K

L




A
SW480
NC
sh-circ-0001944
sh-circ-0001944 +IGFBP1
IGF2BP1
PKM2
β-actin
NC
sh-circ-0001944
sh-circ-0001944+IGFBP1
Relative protein level
1.5
1.0
0.5
0.0
***
***
IGFBP1
PKM2
B
RKO
NC
sh-circ-0001944
sh-circ-0001944 +IGFBP1
IGF2BP1
PKM2
β-actin
NC
sh-circ-0001944
sh-circ-0001944+IGFBP1
Relative protein level
1.5
1.0
0.5
0.0
***
***
IGFBP1
PKM2
C
SW480
NC
sh-circ-0001944
sh-circ-0001944+IGF2BP1
Glucose
2-GD
Oligomycin
ECAR (mpH/min)
500
400
300
200
100
0
0
20
40
60
80
100
Time (minutes)
D
RKO
NC
sh-circ-0001944
sh-circ-0001944+IGF2BP1
Glucose
2-GD
Oligomycin
ECAR (mpH/min)
600
400
200
0
0
20
40
60
80
Time (minutes)
E
SW480
NC
sh-circ-0001944
sh-circ-0001944+IGF2BP1
Oligomycin
FCCP
Rote/AA
OCR (pmol/min)
1000
800
600
400
200
0
0
20
40
60
80
100
Time (minutes)
F
RKO
NC
sh-circ-0001944
sh-circ-0001944+IGF2BP1
Oligomycin
FCCP
Rote/AA
OCR (pmol/min)
1000
800
600
400
200
0
0
20
40
60
80
100
Time (minutes)

Supplementary Files

This is a list of supplementary files associated with this preprint. Click to download.

- OLrawdata.zip